medRxiv preprint doi: https://doi.org/10.1101/2024.07.16.24310501; this version posted July 16, 2024. The copyright holder for this preprint (which was not certified by peer review) is the author/funder, who has granted medRxiv a license to display the preprint in perpetuity. All rights reserved. No reuse allowed without permission.

Brain Imaging Phenotypes Associated With Polygenic Risk For Essential Tremor

Miranda Medeiros[1,2*], Alexandre Pastor-Bernier[2*], Houman Azizi[2,4], Zoe Schmilovich[1,2], Charles-Etienne Castonguay[1,2], Peter Savadjiev[2,3], Jean-Baptiste Poline[2,3], Etienne St-Onge[5], Fan Zhang[6,7], Lauren J. O'Donnell[6], Ofer Pasternak[8,9], Yashar Zeighami,[2,3] Patrick A. Dion[2,3], Alain Dagher[2,3*], Guy A. Rouleau[1,2,3*]

1. Department of Human Genetics, McGill University, Montréal, QC, Canada
2. Montreal Neurological Institute-Hospital, McGill University, Montréal, QC, Canada
3. Department of Neurology and Neurosurgery, McGill University, Montréal, QC, Canada
4. Douglas Mental Health University Institute, McGill University, Montréal, QC, Canada
5. Université du Québec en Outaouais (UQO), Gatineau, QC, Canada
6. Harvard Medical School, Boston, MA, USA
7. School of Information and Communication Engineering, University of Electronic Science and Technology of China, Chengdu, China
8. Department of Psychiatry, Mass General Brigham, Harvard Medical School, Boston, MA, USA
9. Department of Radiology, Mass General Brigham, Harvard Medical School, Boston, MA, USA

[*]Equal contribution

Abstract

Essential tremor (ET) is a common neurological disorder typically characterized by involuntary action tremor of the upper limb. ET has a strong genetic basis that may develop via the additive contribution of risk variants of varying frequencies. About 20% of ET liability can be explained by common variants which are incorporated in polygenic risk scores (PRS) that quantify individual risk level. Magnetic resonance imaging (MRI) has identified subtle abnormalities in the brains of people with ET. In particular, diffusion-weighted magnetic resonance imaging (dMRI) has been used to identify abnormalities in the connectivity and microstructure of white matter tracts in ET patients. In addition, diffusion and T1 MRI also demonstrate abnormalities in grey matter in essential tremor. However, these studies are performed in small samples and do not always replicate. Moreover, the mechanisms by which genetic risk affects the brain to render individuals vulnerable to ET remain unknown. In this study we

NOTE: This preprint reports new research that has not been certified by peer review and should not be used to guide clinical practice.

medRxiv preprint doi: https://doi.org/10.1101/2024.07.16.24310501; this version posted July 16, 2024. The copyright holder for this preprint (which was not certified by peer review) is the author/funder, who has granted medRxiv a license to display the preprint in perpetuity. All rights reserved. No reuse allowed without permission.

probe the vulnerability of healthy people to ET by investigating the association of white matter dMRI, grey matter dMRI and morphometry with ET PRS in close to 30,000 individuals from the UK Biobank (UKB). Our results indicate significant effects of ET PRS on mean diffusivity, a measure of white matter microstructure, in cerebellar input tracts, thalamocortical motor tracts, and premotor and prefrontal white matter. We also found significant associations between ET PRS and grey matter tissue microstructure, in particular the red nucleus, caudate, putamen, and several regions of the motor thalamus, notably the ventral intermediate and ventrolateral nuclei. ET PRS was also associated with reduced grey matter volumes in several cortical and subcortical areas, notably affecting regions with functional projections to the cerebellar dentate nucleus. Further negative associations of ET PRS and grey matter volume were observed in the caudate, putamen, cerebellum and all brainstem subdivisions, including the inferior olivary nucleus, a known arrhythmogenic center in ET. We also found ET PRS associated reductions in volume of the ventral diencephalon, an area that includes the zona incerta, the crus cerebri, the lenticular fasciculus, and the medial lemniscus. The anomalies identified include the entire grey and white matter networks connected to surgical sites effective in treatment of ET. Furthermore, transcriptomic genomic structural equation modeling identified the 17q21.31 locus as relevant to the observed grey matter phenotype. Finally, comparison of low PRS individuals to a small number of patients with ET (N=49) in the UK Biobank revealed that most of the disruptions identified here are also present in ET patients. Altogether these results show that brain structural vulnerabilities in healthy people at risk of developing ET correspond to areas that are also known to be involved in the pathology of ET. High genetic risk of ET seems to disrupt ET brain networks even in the absence of overt symptoms of ET.

Introduction

Essential tremor (ET) is one of the most common movement disorders, affecting more than 60 million people worldwide. It is characterized by action tremor predominantly in the hands, although it can also affect the legs, head, and voice. The prevalence of ET rises with age, and age at diagnosis ranges from childhood to the sixth decade.[1,2] A family history is present in over half of patients, and twin studies demonstrate a concordance rate of 60-90% in monozygotic twins.[1]

ET is thought to be polygenic, and common genetic variants explain over 18% of the susceptibility.[3] The contribution of known common variants in ET can be summed to generate polygenic risk scores (PRS) to quantify individual level risk. The underlying neural cause of ET or its genetic mechanisms remain

medRxiv preprint doi: https://doi.org/10.1101/2024.07.16.24310501; this version posted July 16, 2024. The copyright holder for this preprint (which was not certified by peer review) is the author/funder, who has granted medRxiv a license to display the preprint in perpetuity. All rights reserved. No reuse allowed without permission.

unknown, but evidence from MRI studies and therapeutic effects of neurosurgery points to abnormalities in cerebellar-thalamic circuits.[1]

In this study we calculated a PRS for ET from GWAS summary statistics in 29,706 participants from the UK Biobank (UKB) and combined this with brain imaging phenotypes to map the brain abnormalities underlying vulnerability to ET.[3-5] We used imaging-derived phenotypes (IDP) including white and grey matter dMRI, and cortical and subcortical morphometry to show that common variant driven ET genetic risk is associated with effects in motor-control regions of the brain in healthy individuals.

Specifically, we show that white matter tissue microstructure associations with ET PRS implicate tracts involved in ET pathophysiology. We found associations of ET PRS with grey matter dMRI in the cerebellum, red nucleus, pons, midbrain, medulla and ventral DC incorporating various regions interconnected by the prelemniscal, cortico-pontine and dentato-rubro-thalamic tracts belonging to the Guillain-Mollaret triangle, which is implicated in ET rhythmogenesis.[6] In addition, we found negative associations of ET PRS with grey matter volume in motor regions of the cerebellum as well as areas of the thalamus that are common targets of deep brain stimulation (DBS). We identified cortical and subcortical volume differences between high-risk and low-risk healthy individuals in regions previously implicated in symptomatic ET. Additionally, through structural equation modeling and transcriptomic analysis, we identified a shared transcriptome of imaging derived phenotypes related to ET which points to the 17q21.31 locus of chromosome 17 as being relevant in ET specific cerebellar grey matter volume vulnerabilities.

Though the healthy individuals studied have not developed ET, our results show that their genetic liability is associated with abnormalities in specific brain regions as well as connecting white matter tracts involved in ET. We provide further support for these findings by showing shared vulnerabilities in several brain regions between healthy individuals with the highest genetic risk for ET and people in the UKB diagnosed with ET. These findings demonstrate that ET genetic risk manifests in the brain even in non-symptomatic individuals.

Methods

UK Biobank Data

Publicly available data from the UKB used in this study consist of genetic and MRI data from 42,488 participants.[4] To assure the quality of the data, we excluded individuals with poor image quality,

medRxiv preprint doi: https://doi.org/10.1101/2024.07.16.24310501; this version posted July 16, 2024. The copyright holder for this preprint (which was not certified by peer review) is the author/funder, who has granted medRxiv a license to display the preprint in perpetuity. All rights reserved. No reuse allowed without permission.

specifically relying on the UKB processing pipeline,[7] which identified scans with excessive head motion and artifacts, and participants with visible brain pathology. Individuals with clinical diagnoses associated with brain pathology (International Classification of Diseases (ICD-10): HIV (20:24), neoplasm (69:72), mental (00:09,25,28:31,70:73,78:79), brain disorders including Alzheimer's Disease and Parkinson's Disease (00:14, 20:26, 30:32, 35:37, 40:41, 45:46, 80:83, 91:99), development disorders (00:07, 90:93, 95:99), and brain injury (04, 06:09)) and participants with non-European ancestries, based on principal component analysis (PCA) of the genotypes (UKB field ID: 21006), were excluded. After exclusion criteria 29,706 individuals were included in the white and grey matter diffusion-weighted MRI analysis, and 30,426 individuals in the cortical and subcortical volume analysis. Brain imaging was conducted on Siemens Skyra 3T running VD13A SP4 with a standard Siemens 32-channel RF receive head coil in 3 different centers, Manchester (2015), Newcastle, and Reading (2017). For T1w imaging, 3D MPRAGE, sagittal, in-plane acceleration iPAT=2, prescan-normalise as used. The resolution was 1mm isotropic with a 208x256x256 field-of-view matrix. The duration of the scan was 5 minutes. For diffusion imaging, the resolution was 2mm isotropic, with a 104x104x72 field-of-view matrix. The duration of the scans were 7 minutes, including 36 seconds for phase-encoding reversed data. Five diffusion directions were acquired at b=0 (+3 blip-reversed), and 50 diffusion directions were acquired for two diffusion-weighted shells (b=1000 and b=2000 mm/s2, total of 100 distinct diffusion directions). The gradient timings were δ=21.4 ms, Δ=45.5 ms; Spoiler b-value = 3.3 s/mm 2. SE-EPI with x3 multislice acceleration, no iPAT, fat saturation. The diffusion prepraration was a standard ("monopolar") Stejskal-Tanner pulse sequence.

The set of IDPs used here consisted of brain volume derivatives (from T1-weighted MRI), and dMRI derivatives. IDPs were either calculated and quality-controlled by the UKB and the Centre for Functional MRI of the Brain at the University of Oxford, or by the authors of the present manuscript as described below. T1-weighted structural images (defaced) were used to obtain brain masks using BET (Brain Extraction Tool)[8] and FLIRT (Functional Magnetic Resonance Imaging of the Brain (FMRIB)'s Linear Image Registration Tool),[9,10] was used to register the masked brain to the Montreal Neurological Institute (MNI) 152 2006 non-linear standard-space template. FAST (FMRIB's Automated Segmentation Tool)[11] was used for tissue-type segmentation. FAST was used to generate 139 IDPs, by summing the grey matter partial volume estimates within 139 regions of interest (ROIs). These ROIs are defined in MNI152 space, combining parcellations from several atlases: the Harvard-Oxford cortical and subcortical atlases,[12-15] and the Diedrichsen cerebellar atlas.[16] FreeSurfer modelling v6.0.0 was used to estimate cortical surface.[17-19] Surface atlases were used to extract IDPs of regional cortical surface area, volume and thickness resulting in 66 ROIs.[14,20] Subcortical regions were extracted using FreeSurfer's aseg tool, and

medRxiv preprint doi: https://doi.org/10.1101/2024.07.16.24310501; this version posted July 16, 2024. The copyright holder for this preprint (which was not certified by peer review) is the author/funder, who has granted medRxiv a license to display the preprint in perpetuity. All rights reserved. No reuse allowed without permission.

further segmentation of subcortical regions was carried out.[21] Freesurfer subcortical volumetric measures were obtained for subcortical regions in addition to global brain volume, grey matter, white matter and cerebrospinal fluid (CSF) volumes corresponding to the following UKB IDs: 30710, 26514, 26518, and 26527. 208 ROIs were obtained in the process. All FreeSurfer outputs were quality control checked with the Qoala-T approach by the UKB.[22]

Commonly recommended confound-regressor covariates[23] were incorporated in all GLM (General Linear Model) statistical analyses used in this study: acquisition date (UKB field ID: 21862), age (UKB field ID: 21003), age^2, sex (UKB field ID: 31), age*sex, head motion from rfMRI (UKB field ID: 25741), and head motion from task fMRI (UKB field ID: 25742).

Diffusion Imaging Derivatives

Diffusion-weighted MRI was used to derive microstructural measures from white and grey matter. White matter tractograms and the standard diffusion tensor imaging (DTI) derivatives of fractional anisotropy (FA), mean diffusivity (MD), radial diffusivity (RD), and axial diffusivity (AD) for each UKB participant were computed using the Tractoflow[24] pipeline (Fig. 1A & 1B). The pipeline performs diffusion weighted imaging (DWI) preprocessing steps, including denoising, eddy-top-up, brain extraction, N4 Bias correction, DWI normalization, and resampling to 1mm isotropic spatial resolution. Standard diffusion derivatives are then obtained from dMRI modeling (only b-values under 1,200 mm/s). In parallel, T1 preprocessing, DWI registration (b0), and tissue segmentation are obtained in order to produce inclusion, exclusion and seeding masks for tractography. Tracking then proceeds using the fiber orientation distribution function metrics (fODF) image, the obtained inclusion and exclusion maps, and the white matter seeding mask. The tracking algorithm used was constrained particle filter tracking and a probabilistic method with ten (10) seeds per voxel from the white-matter mask.[25] In addition, free water (FW) was computed in the white matter skeleton (pft_seeding_mask.nii.gz) from Tractoflow[24] output. A Matlab script, FreeWater_OneCase.m was used to perform preprocessing, free water elimination and postprocessing as specified by Pasternak et al.[26] FW is defined as the compartment of water molecules that do not experience flow or diffusion restriction. In the FW model two compartments are represented by two tensors corresponding to a tissue and a water compartment. The tissue compartment follows DTI's formalism.[26,27] The water compartment is modeled by an isotropic tensor with fixed diffusivity of water in body temperature as previously described.[26]

medRxiv preprint doi: https://doi.org/10.1101/2024.07.16.24310501; this version posted July 16, 2024. The copyright holder for this preprint (which was not certified by peer review) is the author/funder, who has granted medRxiv a license to display the preprint in perpetuity. All rights reserved. No reuse allowed without permission.

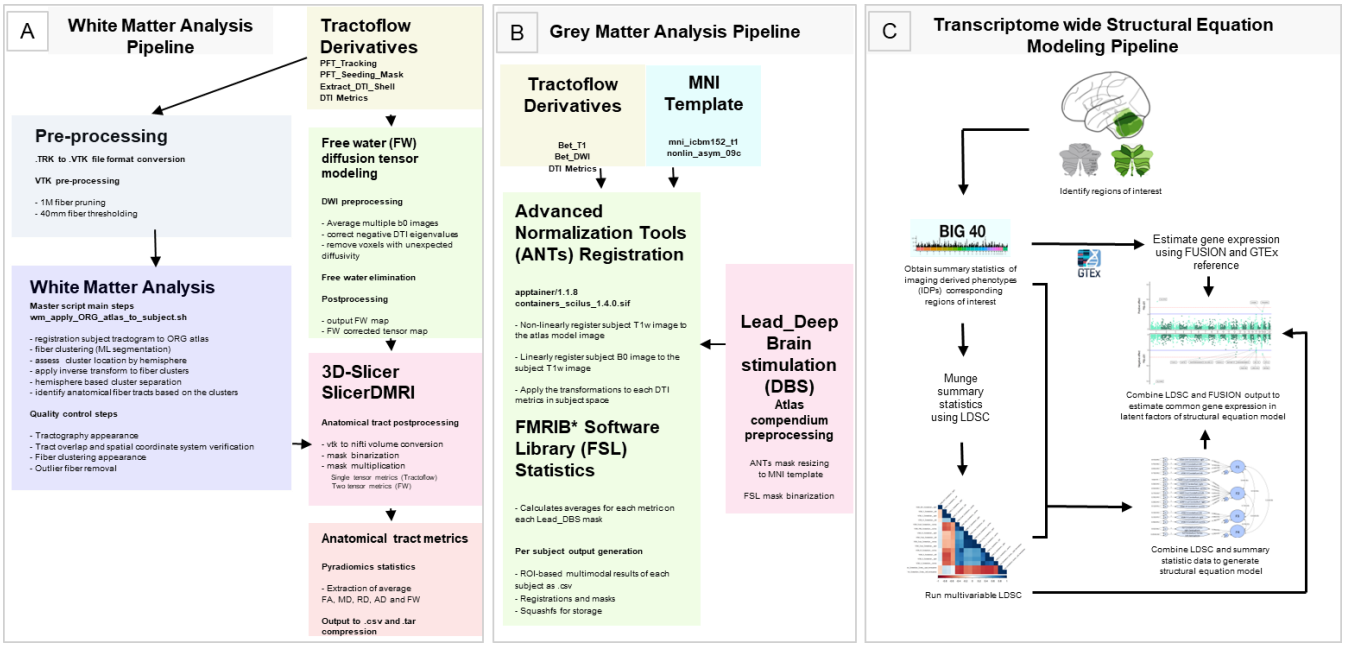

Figure 1. Flowcharts depicting applied methodologies
(A) Flowchart describing the different processing steps of the white matter processing pipeline from tractoflow derivatives to anatomical tract diffusion metrics. (B) Flowchart describing the different processing steps of the grey matter processing pipeline from tractoflow derivatives to grey matter diffusion metrics. (C) Flowchart describing the different steps taken to construct genomic structural equation model (GenomicSEM) and transcriptome wide structural equation model (T-SEM) for gray matter cerebellar imaging derived phenotypes (IDPs). *Functional MRI Bayesian (FMRIB) (Woolrich et al. 2009)

White matter tractograms using 1M streamlines and 4mm fiber-length threshold for each subject were then registered to the O'Donnell Research Group (ORG) anatomically curated atlas.[28] Registration, tract segmentation and average diffusion measure extraction for each tract was obtained via a white matter processing pipeline which uses white matter analysis machine learning for tract segmentation (https://github.com/hayabusapb/wma_qc).[29] ORG atlas segmentation yielded 800 fiber clusters organized into 73 anatomical tracts, including 58 deep white matter tracts, major long-range association and projection tracts, commissural tracts, and tracts related to the brainstem and cerebellar connections.

Grey matter diffusion weighted derivatives were also computed for subcortical structures. To identify relevant subcortical structures, we used the Lead_DBS toolbox, which contains subcortical and white matter atlases used in planning deep brain surgery for neurological conditions such as ET.[30] A compendium atlas of subcortical ROIs was generated and applied to the processed DWI data with a grey matter processing pipeline (https://github.com/HoumanAzizi/UKB_DTI_Pipeline). ROI masks were resized, binarized and registered from atlas space (*ICBM 2009b* non-lin asym.) to subject space as

medRxiv preprint doi: https://doi.org/10.1101/2024.07.16.24310501; this version posted July 16, 2024. The copyright holder for this preprint (which was not certified by peer review) is the author/funder, who has granted medRxiv a license to display the preprint in perpetuity. All rights reserved. No reuse allowed without permission.

described in Fig. 1. The atlases used to generate the subcortical ROIs were: Nigral organization atlas,[31] Essential Tremor Probabilistic Mapping,[32] Essential Tremor Hypointensity,[33] DBS targets,[34] DBS Tractography Atlas,[35] Dystonia Response Tract Atlas,[36] Cerebellar Functional Networks,[36] Atlas of the Human Hypothalamus,[37] TOR-signPD,[38] Thalamic Functional Atlas,[39] TOR-PSM dystonia,[40] Striatal Functional Networks,[41] Brainstem Connectome Atlas,[42] the Zona Incerta Atlas,[43] DISTAL (DBS intrinsic template Atlas),[44] Human Motor Thalamus atlas,[45] Melbourne subcortical atlas,[46] THOMAS (Thalamus optimized multi-atlas segmentation),[47] ABGT (Atlas of Basal Ganglia and Thalamus),[48] AHEAD (Amsterdam Ultra-high field adult lifespan database),[49] HybraPD Atlas,[50] and Xiao's subcortical atlas.[51] Grey matter masks were obtained from each atlas in Lead-DBS. All masks were binarized and registered to the MNI 152 2009c non-linear template. Tractoflow[24] diffusion measures masks in the MNI space were multiplied to each mask and an average FA, MD, RD and AD measure obtained for each ROI.

Polygenic Risk Score Calculation

Full summary statistics from the most recent and largest ET genome-wide association study (GWAS) from Liao *et al*.[3] were used to calculate ET single nucleotide polymorphism (SNP) posterior effect estimates through the PRS-CS tool, which uses Bayesian regression and continuous shrinkage priors to predict genetic disease risk across varying genetic architectures.[5] Using the PLINK *--score* command,[52] SNP posterior effect estimates were summed per genotype at the individual level to generate an ET PRS for all UKB participants in the current study.

ET PRS was calculated for all individuals with both genotyping and MRI data in the 2019 release of UKB, yielding a sample size of 29,706 (white and grey matter diffusion-weighted MRI analysis) and 30,426 (cortical and subcortical volume analysis) individuals after application of previously mentioned exclusion criteria.[23] At the variant level, quality control of the UKB genotyped samples consisted of removing: ambiguous variants (palindromic SNPs with effect allele frequencies between 0.4 and 0.6), variants with imputation information less than 0.4, variants with minor allele frequency less than 0.005, variants that fail Hardy-Weinberg Equilibrium (1×10^{-5}), variants with missingness greater than 0.02, and variants with more than 2 alleles.[53] For sample level quality control of the UKB genotyped samples, individuals with ET (UKB data-field 20002 - Non-cancer illness code=1525) were removed from analysis to focus on non-symptomatic individuals with increased genetic risk for ET. Individuals of European ancestry were retained using UKB ancestry principal components (UKB data-fields: 22009 and 22006) to limit population stratification and to stay consistent with the ET GWAS used.[3] Correct ancestry groupings were verified using the 1000 Genomes Project as reference to ensure remaining

medRxiv preprint doi: https://doi.org/10.1101/2024.07.16.24310501; this version posted July 16, 2024. The copyright holder for this preprint (which was not certified by peer review) is the author/funder, who has granted medRxiv a license to display the preprint in perpetuity. All rights reserved. No reuse allowed without permission.

samples clustered with those of European origin.[54] Principal component analysis (PCA) was done for remaining samples using PLINK to further correct for population stratification.[52] Polygenic scores were then corrected by regressing out the top 15 principal components.

Testing Associations between Imaging Features and ET PRS

GLM were used to evaluate associations between imaging features (imaging derived phenotypes (IDPs): dMRI and morphometry) and ET PRS. The basic GLM for white matter diffusion MRI analysis incorporated a mean diffusion measure (e.g. FA) as dependent variable for each tract, and the Z-score corrected ET PRS along with the previously mentioned confounding covariates (acquisition date, age, age^2, sex, age*sex, head motion from rfMRI and head motion from task fMRI) as independent variables. We used ANOVA type III in R to assess statistical significance for each measure in each tract. FDR-corrected α-threshold for all analyses was set at 0.05. Effect size was assessed with Eta-squared and Cohen's F. The same approach was used for grey matter dMRI analysis in the Lead-DBS subcortical atlas compendium regions.

We investigated the associations between cortical surface area, cortical thickness, cortical and subcortical volume in each ROI with ET PRS using the same GLM approach.[23] To account for intra-cranial volume variability in cortical and subcortical segmentations, we corrected ROIs for total intracranial volume (UKB field ID: 26521-2.0).

Comparison of Genetically High-Risk and Low-Risk Individuals to ET Patients

To better understand the brain correlates of ET genetic risk we made use of the fact that some UKB participants were diagnosed with ET. In total, 49 individuals with ET had an MRI assessment that passed quality control. We then identified a group of control participants from the imaging cohort matched to the ET participants with R MatchIt using GLM and nearest neighbour estimation (Table S24). Full distance matching samples with exact ratio (1:1) were obtained with subcortical ROI volumes as the dependent variable and sex, age, scan date and scanning center as matching covariates. Healthy control groups were also selected according to PRS: matching subgroups were generated from the upper 5% quantile (genetically high-risk PRS) and lower 5% quantile (genetically low-risk PRS). We used Welch

medRxiv preprint doi: https://doi.org/10.1101/2024.07.16.24310501; this version posted July 16, 2024. The copyright holder for this preprint (which was not certified by peer review) is the author/funder, who has granted medRxiv a license to display the preprint in perpetuity. All rights reserved. No reuse allowed without permission.

t-test to assess differences between group means for each ROI as this test is more robust to sample variance differences than t-tests.[55]

Genomic-Structural Equation Models (GenomicSEM) of Cerebellar Grey Matter for Transcriptome Wide Association Study (TWAS)

We then sought to identify genes contributing to the structural differences of brain regions associated to ET genetic risk. We first used genomic-structural equation modeling (GenomicSEM)[56] in an exploratory manner to identify a shared genomic architecture across key brain regions identified above. GenomicSEM acts as an extension of linkage-disequilibrium score regression (LDSC) to calculate genetic correlations between traits using GWAS derived summary statistics.[56,57] Then, we made use of GWASes available from the Oxford Brain Imaging Genetics (BIG40) web server of the IDPs identified in our analysis.[58] This allowed us to calculate the shared genetic relationship between brain structure and ET. The focus of this analysis was limited to cerebellar ROIs since many associations with ET PRS were identified in the cerebellum, and there is suggested evidence of cerebellar dysfunction in ET.[1] Keeping a focused set of IDPs (grey matter volume phenotypes corresponding to brain regions of interest) also helps to generate an identifiable model with adequate loading onto latent factors. Thus, grey matter subcortical volume IDPs of the cerebellum associated to ET PRS (Fig. 6) were used for genomicSEM.[56] To understand the shared genetic relationship between IDPs, we first constructed a model capturing the shared genetic architecture of identified cerebellar subcortical volume IDPs. Then we aimed to identify a shared tissue specific transcriptome for the identified regions through a transcriptome wide association study (TWAS).[56] The genomic model establishes the relationship between cerebellar subcortical volume IDPs of varying degrees of genetic overlap while the TWAS then estimates the tissue expression of genes from shared SNPs defined by the model (Fig. 1C).

Full summary statistics of desired IDPs corresponding to identified ROIs were obtained through the Oxford BIG40 web server.[58] As with the PRS analyses conducted earlier, the individuals represented in these summary statistics shared a common European ancestral background. To prepare the data, the summary statistics were filtered and pre-processed using the munge function,[57] which retains HapMap3 SNPs with a minor allele frequency (MAF) greater than 1%. The major histocompatibility complex (MHC) region was excluded prior to LDSC analysis due to the high degree of LD outliers in this region to avoid unwanted influence on estimates.[56] Information score (INFO) was not available in the brain

medRxiv preprint doi: https://doi.org/10.1101/2024.07.16.24310501; this version posted July 16, 2024. The copyright holder for this preprint (which was not certified by peer review) is the author/funder, who has granted medRxiv a license to display the preprint in perpetuity. All rights reserved. No reuse allowed without permission.

phenotype summary statistics, however, only SNPs of INFO >=0.3 were used in the construction of these imaging-derived phenotypes.[58]

The multivariable LD-Score regression was run using LDSC with the European subsample of the 1000 Genomes phase 3 project to generate a genetic correlation matrix for the set of identified cerebellar grey matter volume IDPs (n=30 IDPs).[54,58] Next, the GenomicSEM pre-packaged common factor model (*commonfactor*) was run using Diagonally Weighted Least Square (DWLS) estimation.[56] In this model, the IDPs representing ROIs of interest were loaded onto a single latent factor, but the fit was poor ($\chi^2(405) =$ 2,666,044; AIC = 2,666,164; CFI = 0.618; SRMR = 0.161). From here, we considered the relationship between the cerebellar lobes and constructed a model which reflected the anatomical divisions of the cerebellum using the GenomicSEM *usermodel* function, fitting a model with factors representing the anterior lobe (F1), posterior lobe (F2), flocculonodular lobe (F3), and the cerebellar cortex hemispheres (F4). This provided an improved fit ($\chi^2(192) = 1{,}427{,}192$; AIC = 1,427,324; CFI = 0.796; SRMR = 0.147) but still needed to be further refined. Only IDPs with factor loadings of > 0.5 were retained, and due to the poor loading of the 'VGM VI Cerebellum left' IDP onto factor F2 and its stronger genetic correlation with the 'VGM V Cerebellum' left and right IDPs, it was moved to factor F1. Additionally, the 'VGM I2IV Cerebellum left' IDP was removed from this model to resolve a Heywood case (when a standardized loading is greater than 1). The resulting fit gave the best model ($\chi^2(98) = 12{,}878.13$; AIC =12,954.13; CFI = 0.922; SRMR = 0.109) with an acceptable CFI (> 0.9) and where all factors had a loading of > 0.5 on their respective factor.[56]

Once the relationship between IDPs had been established, we next sought to understand which genes relevant to cerebellar grey matter volume were commonly transcribed across related ET vulnerability regions. To do this, transcriptome-wide SEM (T-SEM) was employed via GenomicSEM to examine the influence of imputed gene expression from FUSION on the model.[56,59] Univariate summary-based TWAS were conducted using ET GWAS summary statistics and pre-computed gene expression weights of European sample for the cerebellum taken from the Genotype-Tissue Expression project (GTEx v8) multi-tissue expression database.[60] Next, the GenomicSEM *read_fusion* function was used to scale the TWAS coefficients and their standard errors to unit-variance to avoid biased comparisons. Finally, the FUSION summary statistics TWAS outputs and previously obtained multivariable LDSC genetic correlations were combined using the GenomicSEM *commonfactorGWAS* function. In doing this, the relationship between gene expression and the model factors can be estimated to determine which genes are commonly expressed within each factor.[56] In total, 6,077 genes with imputed expression from the

medRxiv preprint doi: https://doi.org/10.1101/2024.07.16.24310501; this version posted July 16, 2024. The copyright holder for this preprint (which was not certified by peer review) is the author/funder, who has granted medRxiv a license to display the preprint in perpetuity. All rights reserved. No reuse allowed without permission.

cerebellum were tested for the F2 factor, and significant genes were defined as having a p-value of < 8.23e-6 after Bonferroni correction. The F2 factor was selected because it consists of posterior lobe, the part of the cerebellum involved in fine motor coordination.

Results

Associations Between ET PRS and White Matter Microstructure in Cerebellar and Cortical Tracts

ET PRS was positively associated with MD in many white matter tracts in the ORG atlas (Table S1).[61] Fig. 2 shows the associations of ET PRS and MD in the anterior corpus callosum (CC1; p_{FDR}=0.022), middle cerebellar peduncle (MCP; p_{FDR}=0.021), intracerebellar input and Purkinje tract (left Intra-CBLM-I&P; p_{FDR}=0.037), superficial frontal tract (Sup-F; p_{FDR}=0.03), and left cortico-spinal tract (CST, p_{FDR}=0.042). Weakly positive significant and borderline non-significant associations were also found between ET PRS and MD in the uncinate fasciculus (right UF; p_{FDR}=0.038; left UF, p_{FDR}=0.053) and the left and right superior occipital tracts (Sup-O; p_{FDR}=0.039, Sup-O; p_{FDR}=0.059). Histograms exemplifying the coefficients of these associations can be seen in Fig. S1. ET PRS associations with FW were similar to the associations with MD (Table S1-S2), although cerebellar associations with FW were more strongly significant than with MD in the left and right Intra-CBLM-I&P (p_{FDR}=0.002 and p_{FDR}=0.001), MCP (p_{FDR}<0.001) and the left and right intracerebellar parallel tracts Intra-CBLM-PaT (p_{FDR}=0.022, p_{FDR}=0.013). Frontal, occipital and cortico-spinal projection tracts also showed significant relationships between FW and ET PRS: left Sup-F (p_{FDR}=0.005), left and right Sup-O (p_{FDR}=0.026, p_{FDR}=0.006) and left CST (p_{FDR}<0.042; Fig. S1-2, Table S2). Extended dMRI analysis (Fig. S1, Tables S3-5) revealed that ET PRS was positively associated with RD in the MCP (p_{FDR}=0.014, Table S4) and the left Intra-CBLM-I&P (p_{FDR}=0.038), the cingulum bundle (CB; p_{FDR}=0.015), the CC1 (p_{FDR}=0.016), left and right Sup-F (p_{FDR}=0.007, p_{FDR}=0.027), as well as the bilateral uncinate fasciculus (left UF p_{FDR}=0.028; right UF p_{FDR}=0.038). Borderline significant associations between ET PRS and RD were observed in the bilateral Sup-O (left and right p_{FDR}<0.047) and the inferior occipitofrontal fasciculus (left and right IOFF; p_{FDR}<0.05). ET PRS was positively associated with AD in the striato-parietal (SP; p_{FDR}<0.016; Table S5), superficial-parietal-occipital (Sup-PO; p_{FDR}<0.003), the CC1 (p_{FDR}<0.032), and the right inferior longitudinal fasciculus (ILF; p_{FDR}<0.037; Table S5). We also observed statistically significant negative associations of ET PRS with FA in the left superficial frontal tract Sup-F (p_{FDR}<0.02;

medRxiv preprint doi: https://doi.org/10.1101/2024.07.16.24310501; this version posted July 16, 2024. The copyright holder for this preprint (which was not certified by peer review) is the author/funder, who has granted medRxiv a license to display the preprint in perpetuity. All rights reserved. No reuse allowed without permission.

Table S3). In sum, ET PRS was associated with increased measures of diffusivity and free water, indicating altered tissue microstructure in several white matter tracts implicated in control of movement.

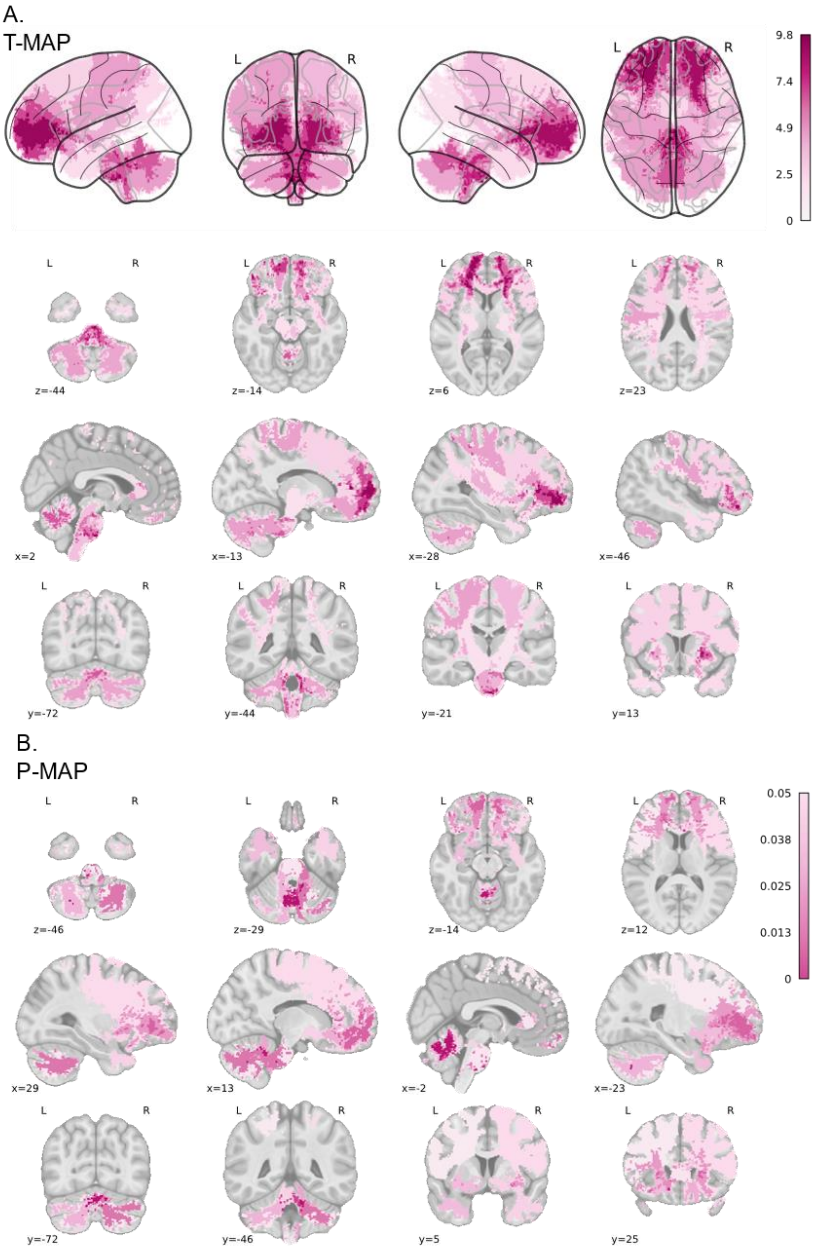

Figure 2. White matter diffusion-weighted magnetic resonance imaging mean diffusivity in O'Donnell Research Group Atlas

Mean diffusivity (MD) across white matter anatomical tracts reveals positive associations with ET polygenic risk scores in cerebellar spinal and frontal projection tracts (O'Donnell Research Group (ORG) anatomically curated fiber clustering atlas, Zhang et al., 2018) (A) Glassbrain representations of the t-statistic projections indicate stronger positive associations in the anterior frontal lobe and cerebellum. A mosaic representation of the t-statistic in the Montreal Neurological Institute (MNI) template MNI152_nlin_asym_09 and axial, transverse and coronal slices is shown below. (B) A mosaic representation of the FDR adjusted p-value projections indicate stronger positive associations in the cerebellar and bilateral frontal lobe projections

medRxiv preprint doi: https://doi.org/10.1101/2024.07.16.24310501; this version posted July 16, 2024. The copyright holder for this preprint (which was not certified by peer review) is the author/funder, who has granted medRxiv a license to display the preprint in perpetuity. All rights reserved. No reuse allowed without permission.

Associations Between ET PRS and Red Nucleus and Thalamus Grey Matter Microstructure

To confirm neuroanatomical findings known for ET, we ran associations between dMRI measures in the grey matter in targets based on the Lead DBS neurosurgical atlases. We identified regions implicated in the therapeutic effects of deep brain stimulation (DBS) in ET with structural and functional segmentations. We found significant positive associations of ET PRS with FA in the red nucleus bilaterally (RN; left $p_{FDR}<0.0025$ and right $p_{FDR}=0.003$; Table S6; Lead-DBS Essential Tremor Probabilistic Mapping Atlas,[31] Essential Tremor Hypointensity Atlas,[33] RN in the Atlas of the Human Hypothalamus,[37] and in Xiao 2019 subcortical segmentation).[51] The coefficients are shown in Fig. S3, along with MNI_152 projections in Fig. S4. We also found borderline significant negative associations of ET PRS with FA in the caudate ($p_{FDR}<0.056$) and negative associations in Kumar's functional thalamus segmentation in area 7 ($p_{FDR=}0.048$; Kumar Atlas[39]; Fig. S5; Table S10). Conversely, ET PRS had strong positive associations with MD in Kumar's functional thalamus segmentation (posterior and ventral thalamic nuclei; functional areas 3R, 4B_L, 7_L, 13A, bilateral 14, 15R; $p_{FDR}<0.034$).[39] The ET PRS was also weakly associated with MD in the right periventricular hypothalamic nucleus ($p_{FDR}<0.049$; Table S11) and the left hippocampus ($p_{FDR}<0.035$; Table S7, Fig. S5). The t-statistic projections in Fig. S5 show stronger associations in bilateral posterior and ventral thalamic nuclei. These associations of ET PRS with the functional thalamic network and the hypothalamus were also observed in extended dMRI measures: radial diffusivity (RD) and axial diffusivity (AD) in both regions (Tables S12-13). We found no significant associations of ET PRS in any diffusion measures for Zhang's 2017 substantia nigra segmentation[31] or Buckner's 2011 functional Cerebellum[62] (Tables S6-7 & Table S11).

To further refine neuroanatomical localization of these effects in striatum, thalamus and basal-ganglia we investigated ET PRS associations in the following atlases: DISTAL,[44] Human Motor Thalamus atlas,[45] Melbourne subcortical atlas,[46] THOMAS,[47] ABGT,[48] and AHEAD.[49] We projected the MD ET PRS association t-statistic and adjusted MD ET PRS association p-values on the MNI2009c non-linear template. We found significant positive associations of ET PRS with MD throughout the thalamus (Table S14), in particular within a stripe of the bilateral ventro lateral nucleus (VL; Human Motor Thalamus atlas)[45] encompassing the ventro-medius externus, zentro-lateralis externus, ventralis intermediate nucleus (VIM), the dorso-intermedius externus nucleus and dorso-oralis internus (DISTAL).[44] Left hemisphere unilateral associations with the medial dorsal, ventro-caudal, zentro-caudalis and the

medRxiv preprint doi: https://doi.org/10.1101/2024.07.16.24310501; this version posted July 16, 2024. The copyright holder for this preprint (which was not certified by peer review) is the author/funder, who has granted medRxiv a license to display the preprint in perpetuity. All rights reserved. No reuse allowed without permission.

lateropolaris nuclei were also observed. Modest associations were also identified bilaterally in the habenula (left hemisphere p_{FDR}=0.026; Fig. 3). We also identified particularly strong negative ET PRS associations with FA in the body and anterior extent of the caudate nucleus, in particular the medial caudate (mCAU), the dorsal anterior Caudate (Caudate-DA) in addition to the nucleus accumbens in the Melbourne subcortical atlas (Fig. 4).[46] Negative associations were also observed between FA in the ventral posterior thalamus and the pedunculo pontine nucleus (p_{FDR}=0.057), a DBS stimulation area normally used for treating tremor in Parkinson's Disease (PD) (Fig. 4; Table S15).[63] In summary, regions that are normally associated with essential tremor vulnerability were found to be positively associated with MD and negatively associated with FA, with exception to the red nucleus for which we observed a positive ET PRS association with FA across several atlases in Lead_DBS.

medRxiv preprint doi: https://doi.org/10.1101/2024.07.16.24310501; this version posted July 16, 2024. The copyright holder for this preprint (which was not certified by peer review) is the author/funder, who has granted medRxiv a license to display the preprint in perpetuity. All rights reserved. No reuse allowed without permission.

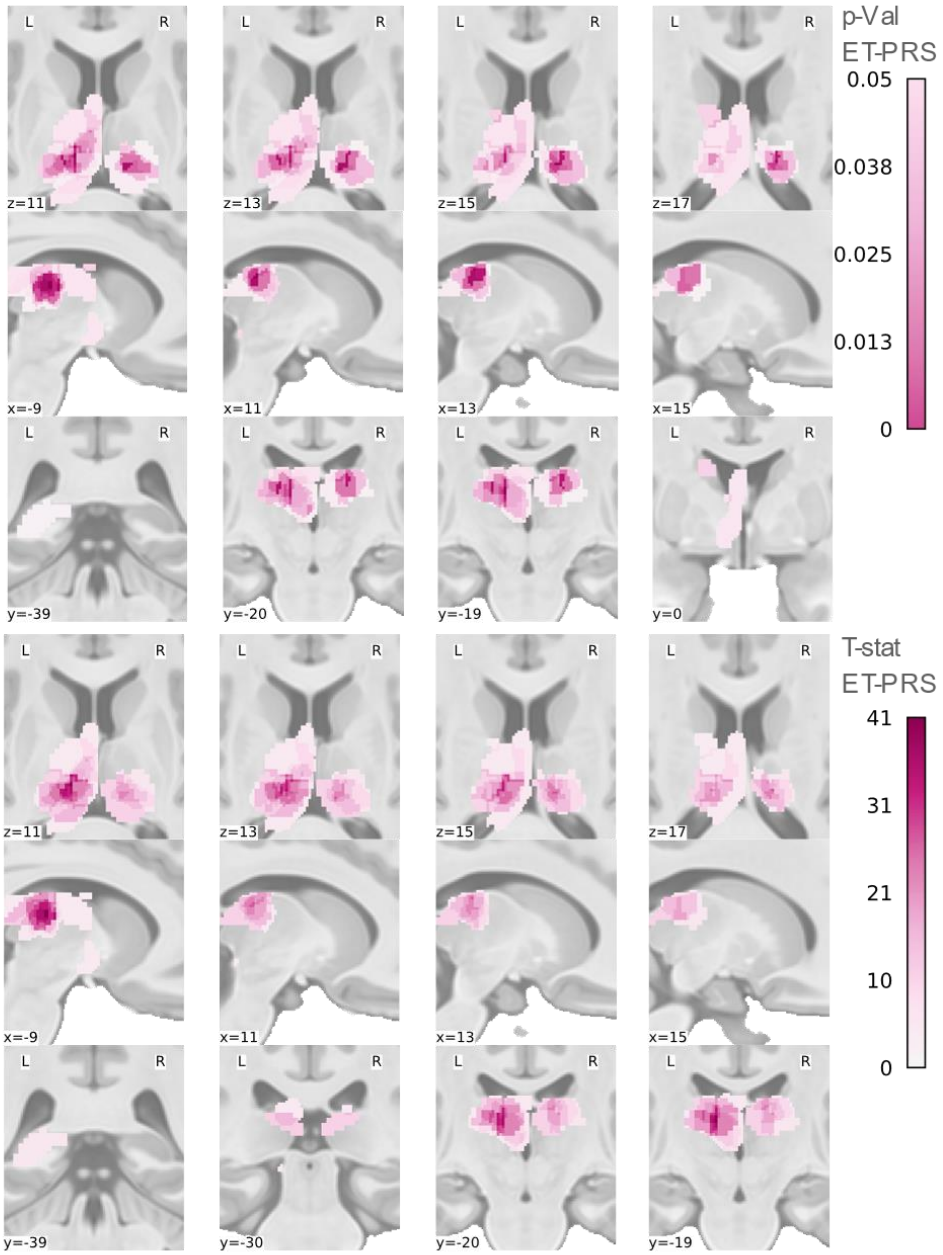

Figure 3. Grey matter diffusion-weighted magnetic resonance imaging mean diffusivity of thalamic regions of the Ilinsky and DISTAL atlases

ET polygenic risk score associations with mean diffusivity (MD) in each thalamic region of the Ilinsky (Ilinsky et al., 2018) and DISTAL atlas (Ewert et al., 2017). Associations are strongest in the ventral posterior nuclei including ventral intermediate nucleus (VIM). FDR adjusted p-Value projections (above) and T-statistic projections (below).

medRxiv preprint doi: https://doi.org/10.1101/2024.07.16.24310501; this version posted July 16, 2024. The copyright holder for this preprint (which was not certified by peer review) is the author/funder, who has granted medRxiv a license to display the preprint in perpetuity. All rights reserved. No reuse allowed without permission.

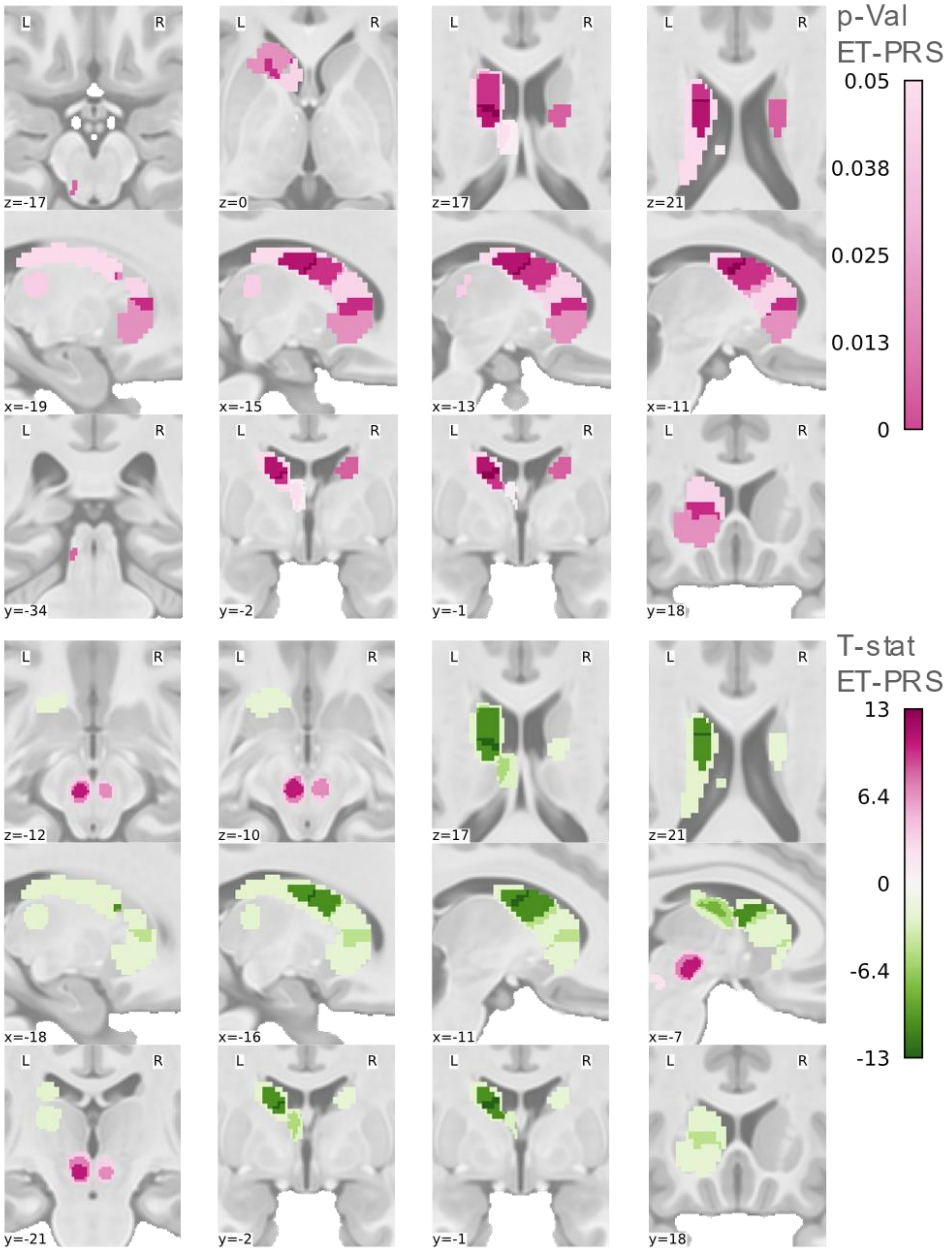

Figure 4. Grey matter diffusion-weighted magnetic resonance imaging fractional anisotropy of caudate, red nucleus, and pedunculopontine nucleus from Ilinsky and Melbourne atlases
ET polygenic risk score (PRS) negative associations with fractional anisotropy (FA) in the caudate are strongest in the body and anterior extent of the caudate. Positive associations with ET PRS can be observed in the bilateral red nucleus. Striatal regions derived from Ilinsky (Ilinsky et al., 2018) and Melbourne subcortical atlases (Tian et al, 2020), FDR adjusted p-Value projections (above) and T-statistic projections (below).

medRxiv preprint doi: https://doi.org/10.1101/2024.07.16.24310501; this version posted July 16, 2024. The copyright holder for this preprint (which was not certified by peer review) is the author/funder, who has granted medRxiv a license to display the preprint in perpetuity. All rights reserved. No reuse allowed without permission.

ET PRS Associations with Cortical Surface Area, Cortical Thickness and Cortical Volume

We found limited associations of ET PRS and cortical surface area, with weak but significant positive associations in the bilateral lateral occipital ($p_{FDR}<0.037$), left inferior parietal ($p_{FDR}<0.038$) and right precentral area ($p_{FDR}<0.047$; Table S18). We observed many associations of ET PRS with cortical volume (Table S19; Fig. 5A), with strongly negative associations in the following ROIs: the bilateral superior parietal ($p_{FDR}<0.0014$), the bilateral caudal middle frontal ($p_{FDR}<0.021$), the bilateral precuneus ($p_{FDR}<0.022$), the left cuneus ($p_{FDR}<0.017$), the left posterior cingulate ($p_{FDR}<0.017$), the rostral middle frontal ($p_{FDR}<0.03$) and borderline significance in the left pars triangularis ($p_{FDR}<0.051$). In contrast, we found no associations of ET PRS with cortical thickness, except borderline significance in the right superior frontal area ($p_{FDR}<0.045$; Table S20).

medRxiv preprint doi: https://doi.org/10.1101/2024.07.16.24310501; this version posted July 16, 2024. The copyright holder for this preprint (which was not certified by peer review) is the author/funder, who has granted medRxiv a license to display the preprint in perpetuity. All rights reserved. No reuse allowed without permission.

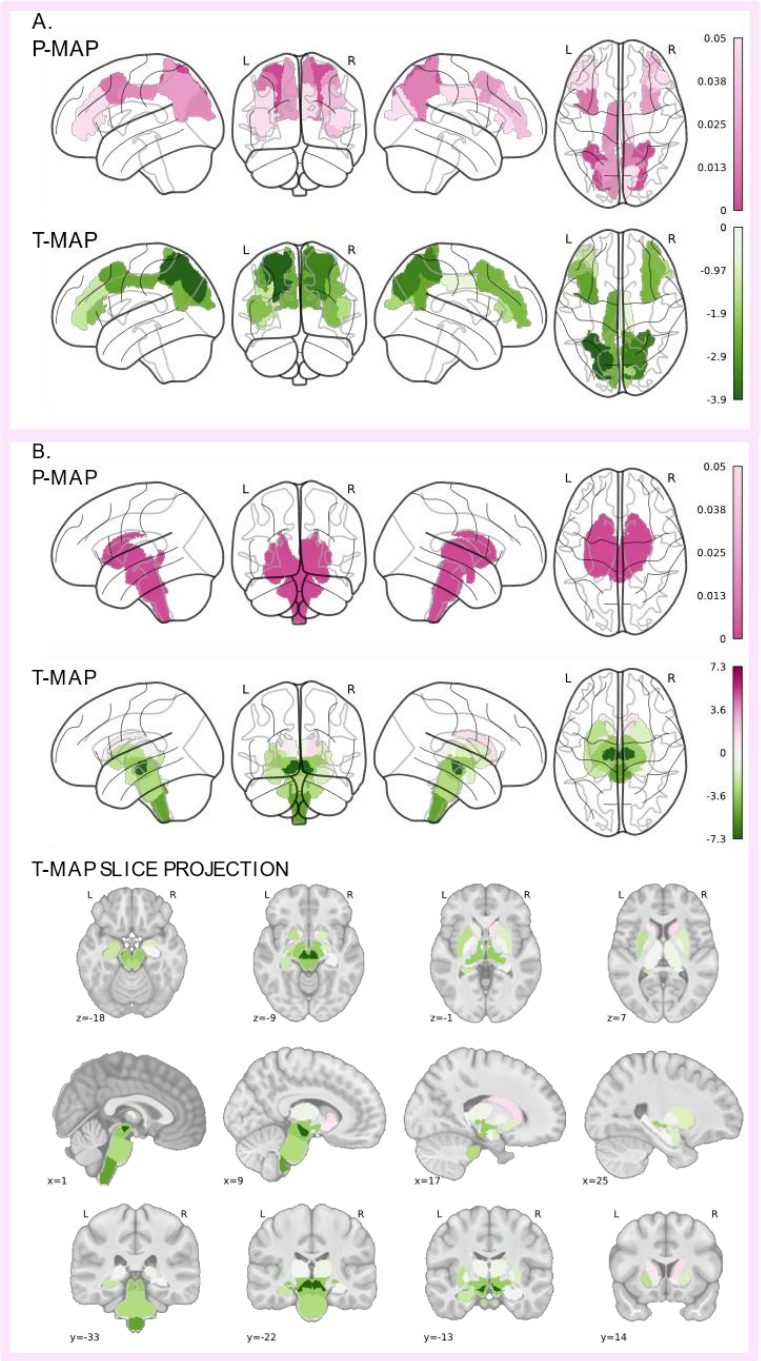

Figure 5. Effect of ET PRS on grey matter cortical, subcortical, brainstem and ventral diencephalon volumes

ET polygenic risk score (PRS) associations are found in the red nucleus (RN) and caudate as well as negative associations in brainstem volume phenotypes. (A) Fractional anisotropy (FA) in RN and caudate (Lead-DBS Essential Tremor Probabilistic Mapping Nowacki 2022, and Essential Tremor Hypointensity, Neudorfer 2022) showing significant associations with ET PRS. (B) Glassbrain FDR adjusted p-Value projections of significant regions associated in the brainstem, such as the midbrain, pons, medulla and ventral diencephalon, as well as the bilateral subcortical structures caudate and putamen (above). Glassbrain representations of the t-statistic projections indicate stronger positive associations in the posterior and ventral thalamic nuclei (middle). T-statistics in the MNI 152_nlin_asym_09 template and axial, transverse and coronal slices (below).

medRxiv preprint doi: https://doi.org/10.1101/2024.07.16.24310501; this version posted July 16, 2024. The copyright holder for this preprint (which was not certified by peer review) is the author/funder, who has granted medRxiv a license to display the preprint in perpetuity. All rights reserved. No reuse allowed without permission.

Associations of ET PRS with Brainstem and Cerebellum Volumes

Our analysis of UKB subcortical volume phenotypes (208 ROIs) showed negative associations with ET PRS in the brainstem (p_{FDR}<5.3e-4) and all its subdivisions, the midbrain (p_{FDR}<0.001), pons (p_{FDR}=0.0079), medulla (p_{FDR}<0.001; Tables S21-23), including the bilateral ventral diencephalon (ventral_DC; p_{FDR}< 0.001; Table S23, Fig. 5B). The ventral_DC refers to a "miscellaneous" area that includes the hypothalamus, mammillary body, subthalamic nuclei, substantia nigra, red nucleus, lateral geniculate nucleus (LGN), medial geniculate nucleus (MGN), zona incerta, lenticular fasciculus, and the medial lemniscus. We also found negative ET PRS associations with subcortical volume in the left putamen (p_{FDR}<0.011) and the left amygdala (p_{FDR}<0.024; Table S22; Fig. 5B). Importantly, we found extensive negative associations of the ET PRS with cerebellar volume (Tables S22-23). Fig. 6 shows the t-statistic projections of these associations in the left cerebellum (p_{FDR}<0.002) right cerebellum (p_{FDR}<0.02), including the bilateral cerebellar white matter (p_{FDR}<0.0023). We found specific associations in the following cerebellar subdivisions: left Crus I (p_{FDR}<0.022), bilateral Crus II (p_{FDR}<0.005), bilateral VI (p_{FDR}<0.001), vermis VI (p_{FDR}<0.005), bilateral VIIb (p_{FDR}<0.022), vermis VIIb (p_{FDR}<0.022), bilateral VIIIa (p_{FDR}<0.029), the bilateral VIIIb (p_{FDR}<0.001), vermis of VIIIb (p_{FDR}<0.013), bilateral IX (p_{FDR}<0.001), vermis IX (p_{FDR}<0.0026) and vermis of X (p_{FDR}<0.001). We found borderline effects in other subcortical regions like the left hippocampus (p_{FDR}<0.03), specifically in the volume of the whole left hippocampal head (p_{FDR}<0.045) and the molecular layer of the left hippocampal head in particular (p_{FDR}<0.013). Among other areas of interest in the extended subcortical segmentation there were negative associations in the left and right temporo-occipital division of the inferior temporal gyrus (p_{FDR}<0.018) and the left insular cortex (p_{FDR}<0.04; Table S22).

medRxiv preprint doi: https://doi.org/10.1101/2024.07.16.24310501; this version posted July 16, 2024. The copyright holder for this preprint (which was not certified by peer review) is the author/funder, who has granted medRxiv a license to display the preprint in perpetuity. All rights reserved. No reuse allowed without permission.

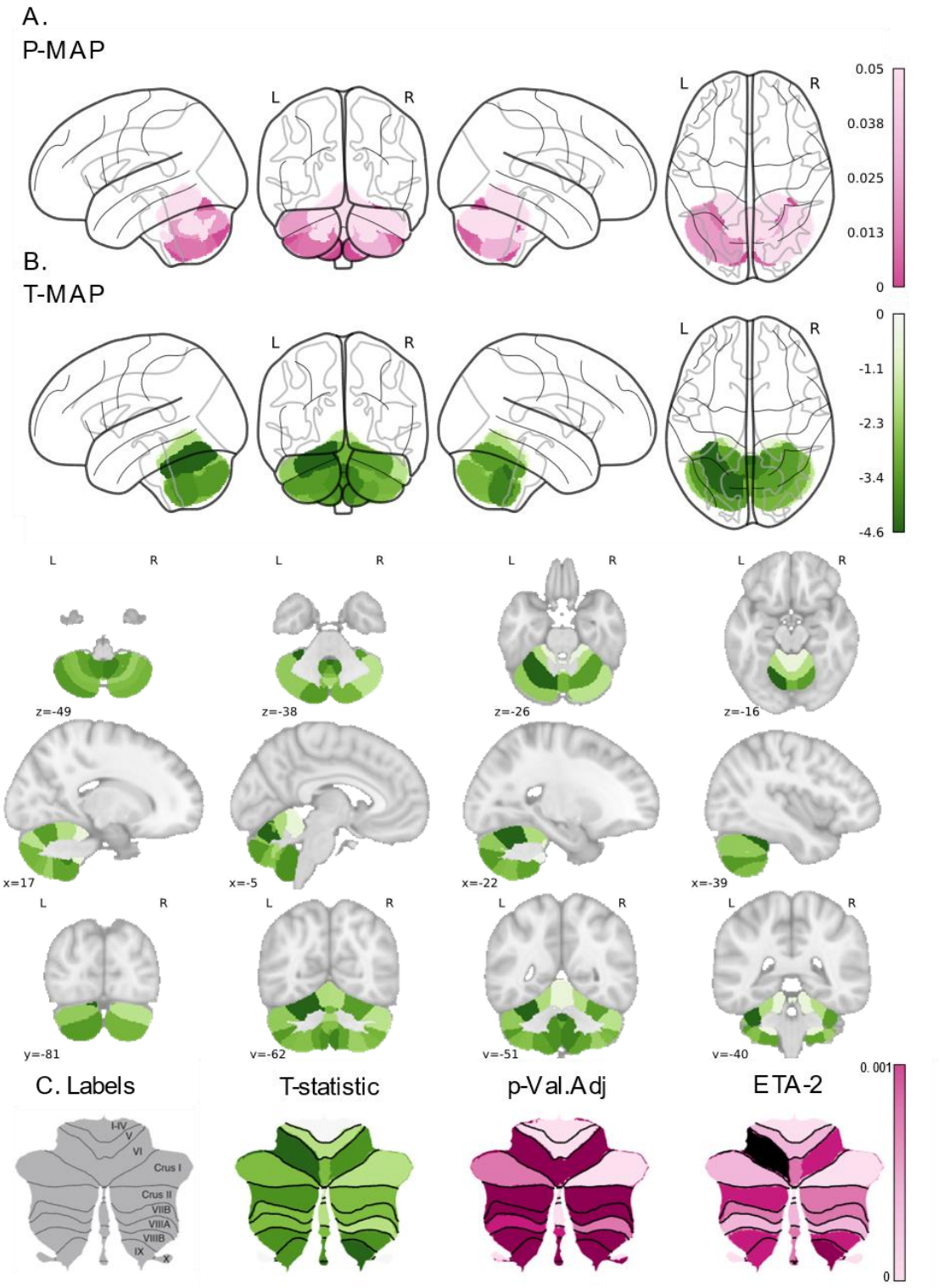

Figure 6. Effect of ET PRS on cerebellar volumes

Cerebellar volumes are negatively associated with ET polygenic risk score (PRS). (A) Glassbrain FDR adjusted p-Value projections. (B) Glassbrain t-statistic and MNI 152 2006 statistic projections (C) Diedrichsen's flatmap statistic projections, illustrating T-statistic, FDR adjusted p-Value and ETA2 effect size projections (Diedrichsen, J., 2006. A spatially unbiased atlas template of the human cerebellum. NeuroImage 33, 127-138)

medRxiv preprint doi: https://doi.org/10.1101/2024.07.16.24310501; this version posted July 16, 2024. The copyright holder for this preprint (which was not certified by peer review) is the author/funder, who has granted medRxiv a license to display the preprint in perpetuity. All rights reserved. No reuse allowed without permission.

Distinct Grey Matter Volume Differences are Observed Between ET Patients and Healthy Controls with Low and with High Genetic Risk for ET

We next compared brain morphology between people diagnosed with ET and matched control participants in the UKB (N=49, 1:1, Table S24). We found lower grey matter subcortical volume in ET patients versus matched genetically low-risk PRS healthy controls (Fig. 7A) in the motor cerebellar regions described in Table S25 (Diedrichsen Atlas).[16] Lower grey matter volume was also found in the whole brainstem, left pallidum, right thalamus, and additional cortical regions in ET vs low-risk PRS (Table S32). Higher subcortical volume between ET and low-risk PRS was found in four cortical areas: the inferior division of the left lateral occipital cortex, the subcallosal cortex, the right orbitofrontal cortex, the right pars orbitalis, and the occipital fusiform gyrus (Table S25).

The grey matter volume differences between ET patients and genetically high-risk PRS healthy controls (Fig. 7B) were much less extensive, weaker, and unilateral in the following cerebellum areas: right VIIIa, left I2IV, and vermis Crus I (Table S25). Lower grey matter subcortical volume between ET and high-risk PRS was observed in the Putamen bilaterally, right Pallidum, bilateral hippocampus (Table S32). Lower cortical volume between ET patients and high-risk PRS was also observed in the parahippocampal cortex, the left middle temporal cortex, the left superior parietal cortex, and the right fusiform cortex (Table S25). Higher cortical volume was found in the bilateral medial orbitofrontal cortex (Table S32).

medRxiv preprint doi: https://doi.org/10.1101/2024.07.16.24310501; this version posted July 16, 2024. The copyright holder for this preprint (which was not certified by peer review) is the author/funder, who has granted medRxiv a license to display the preprint in perpetuity. All rights reserved. No reuse allowed without permission.

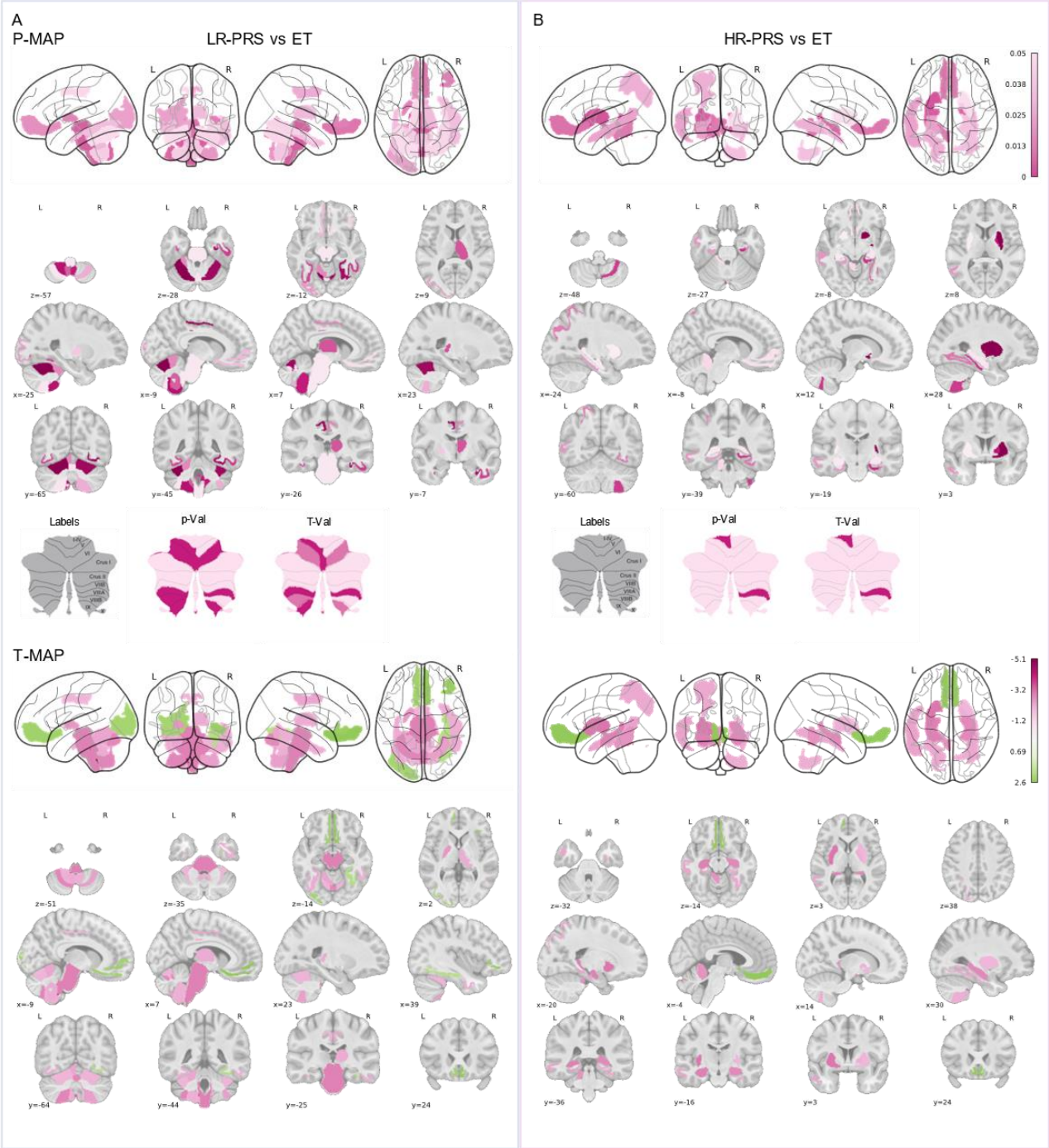

Figure 7. Cortical and subcortical volume differences between ET patients and low and high risk healthy controls

Cortical and subcortical volume differences between (1:1) matched ET patients and healthy controls (HC) (N:49) reveal regions normally associated with ET pathophysiology. These differences are more prominent in the ET vs low-risk (LR) polygenic risk score (PRS) group. The projections of t-statistics (above) and pFDR (below). (A) Regions with negative volume associations in ET patients vs the HC group LR ET PRS. Extensive differences were found in the motor regions of cerebellum, brainstem and thalamus. (B) Fewer negative volume associations comparing ET vs HC group high-risk (HR) ET-PRS. Distinct areas in the orbitofrontal, corpus callosum, and occipital lobes have lower volume in both HC compared to ET.

medRxiv preprint doi: https://doi.org/10.1101/2024.07.16.24310501; this version posted July 16, 2024. The copyright holder for this preprint (which was not certified by peer review) is the author/funder, who has granted medRxiv a license to display the preprint in perpetuity. All rights reserved. No reuse allowed without permission.

Transcriptome-wide Structural Equation Modeling (T-SEM) Identifies Genes Associated with ET

To evaluate genes relevant to ET brain morphometry, GenomicSEM was implemented for transcription-wide structural equation modeling (T-SEM) use. Specifically, we focused on grey matter vulnerability of the cerebellum due to the availability of genetic data and the increasing evidence that cerebellar dysfunction is linked to ET.[1] Cerebellar volume imaging derived phenotypes (IDPs) from the Oxford Brain Imaging Genetics server (BIG40)[58] containing GWAS results corresponding to identified ROIs were used to fit a structural equation model representing genetic vulnerabilities of ET. Cerebellar gene expression estimates for the 16 cerebellar IDPs used in the model (cerebellar lobule grey matter volumes of: I2IV right, V left, V right, VI left, CrusII vermis, VI right, VIIIb vermis, CrusI left, CrusI vermis, Crus I right, IX vermis, X left, X right, X vermis. Subcortical volume of left and right cerebellum cortex hemispheres) from the solved structural equation model (Fig. 8A) described in the methods were obtained through GTEx.[60] IDP factor loadings were generally large and significantly associated with their respective factor. The factor F2 was of interest since it consisted of IDPs of the posterior lobe, which is involved in fine motor coordination. To determine the association between gene expression and the factor, 6,077 genes expressed in the cerebellum were tested. Of the tested genes in the F2 transcriptomic analysis, 16 were significant after Bonferroni correction (p-value < 8.23e-6; Fig. 8B): *SLC44A5, SLC27A3, FOXO3, WASHC3, ZBTB32, ENSG00000258308, UPK1A, PROSER3, ARL17A, COX6B1, KMT5A, LRRC37A2, FAM215B, ENSG00000266918, MAPK8IP1P1, GOLGA6L10* (Table S26; Fig. 8B). Five of these genes belong to the chromosome 17q21.31 region. Of the genes significantly associated to the F2 factor, it is worth noting that only *SLC44A5* displayed a significant degree of heterogeneity, suggesting that its expression is not entirely influenced by the F2 factor alone.

medRxiv preprint doi: https://doi.org/10.1101/2024.07.16.24310501; this version posted July 16, 2024. The copyright holder for this preprint (which was not certified by peer review) is the author/funder, who has granted medRxiv a license to display the preprint in perpetuity. All rights reserved. No reuse allowed without permission.

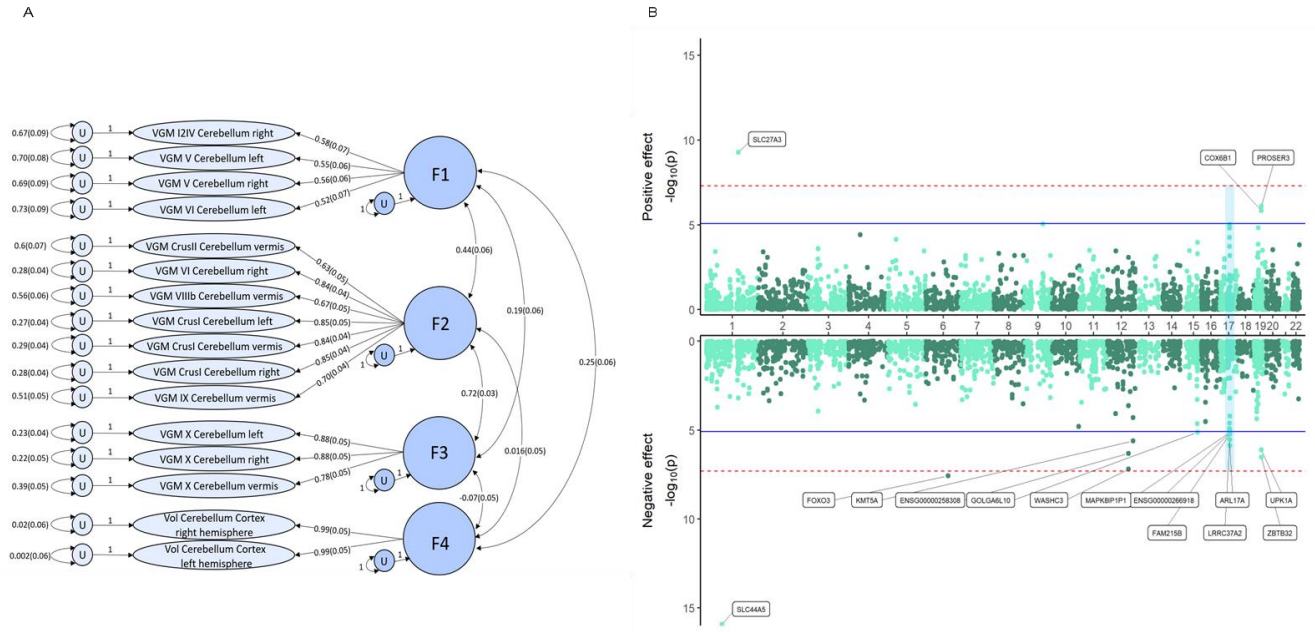

Figure 8. Shared transcriptomics of cerebellar posterior lobe grey matter volumes (latent variable F2)

Genetic structural equation modeling of identified cerebellar imaging-derived phenotypes (IDPs) and integration of cerebellar transcriptomics of factor F2 are depicted as follows. The F2 factor is selected because it consists of posterior lobe (part of the cerebellum involved in fine motor coordination) phenotypes. (A) Path diagram representing factor model of cerebellar IDPs associated with ET with standardized genetic loadings and standard error reported. Factor F1 largely contains anterior lobe IDPs, F2 contains posterior IDPs, F3 contains flocculonodular lobe IDPs, and F4 contains cerebellar cortex hemisphere IDPs. (B) Miami plot of factor F2 (posterior lobe IDPs) showing significant genes from transcriptome-wide structural equation modeling. Associations between gene expression in the cerebellum and factor F2 built from IDPs corresponding to identified cerebellar ROIs are shown. Horizontal blue lines show the Bonferroni significant threshold (p-value: 8.23e-6), red line denotes genome-wide significance threshold, the light blue vertical highlight depicts the 17q21.31 locus.

Discussion

We describe the neuroanatomical correlates of genetic risk for ET in a sample of approximately 30,000 healthy adults. We identified widespread effects of ET PRS on white matter microstructure and subcortical grey matter volume in areas implicated in movement control and therapeutic effects of ET neurosurgery. Specifically, with increasing PRS, there were widespread increases in MD in cerebellum and cerebellar outflow tracts, as well as frontal white matter tracts originating in motor, prefrontal and orbitofrontal cortex. Diffusion-weighted MRI also demonstrated reduced FA in several subcortical nuclei (striatum and thalamus), but significantly increased FA in bilateral red nucleus, in association with higher ET PRS. Grey matter volume was reduced in several cortical areas, and in widespread cerebellar and

medRxiv preprint doi: https://doi.org/10.1101/2024.07.16.24310501; this version posted July 16, 2024. The copyright holder for this preprint (which was not certified by peer review) is the author/funder, who has granted medRxiv a license to display the preprint in perpetuity. All rights reserved. No reuse allowed without permission.

thalamic regions implicated in motor control, with increasing genetic risk. Patients with ET in the same database demonstrated reduced cerebellar and brainstem volumes compared to low and high PRS controls, in the same regions implicated in the PRS analysis. TWAS identified genes associated with cerebellar volume loss, notably in the chromosome 17q21.31 region. Taken together, these results shed light on the mechanism by which genetic risk for ET confers vulnerabilities in neural circuits implicated in tremor generation. We propose that neurodevelopmental effects of ET genes may lead to subclinical alterations in these circuits, rendering them vulnerable to environmental triggers that can lead to overt tremor.

White Matter dMRI Associations Implicate Tracts Involved in ET Pathophysiology

In white matter, a greater genetic risk for ET was associated with widespread increases in MD including the corpus callosum, external capsule, posterior thalamic radiation, cingulum, and uncinate fasciculus. There were also several tracts showing increased MD in the cerebellum: the middle cerebellar peduncle, the intracerebellar input and Purkinje tract. White-matter microstructural changes in tracts involved in primary and associative motor function including the cerebellum have been documented in ET patients.[64-66] These cerebellar white matter alterations are consistent with post-mortem structural changes in cerebellar Purkinje cells and their axons, and neighbouring neuronal populations.[67-69] Our results suggest that similar white matter alterations may also be present in association with genetic risk of ET. In addition to cortical and cerebellar tracts implicated in motor control, we also observed MD alterations in other regions, notably in orbitofrontal and prefrontal white matter. Increased MD in these non-motor tracts were also reported previously in a dMRI comparative study of ET patients versus healthy controls.[64] In small studies, increased MD in non-motor tracts in ET has also been related to subtle cognitive dysfunction.[70] In sum, we find evidence of disrupted white matter microstructure in pathways implicated in the pathophysiology of ET of the cerebellar-brainstem-thalamus- motor cortex axis. However, our results suggest that ET genetic risk also affects white matter tracts beyond those that directly underpin movement control.

Grey Matter dMRI Associations Implicate Regions Involved in ET Pathophysiology

medRxiv preprint doi: https://doi.org/10.1101/2024.07.16.24310501; this version posted July 16, 2024. The copyright holder for this preprint (which was not certified by peer review) is the author/funder, who has granted medRxiv a license to display the preprint in perpetuity. All rights reserved. No reuse allowed without permission.

The thalamic ventral intermediate nucleus (VIM) is one of the most common targets for DBS and ablative therapy in ET.[33] Explicit ET PRS associations within this area and nearby hot zones (e.g. zona incerta; ZI) were found both in FA and MD measures in our study using several atlases designed for surgical planning.[39,44-49] Associations of GM dMRI (FA, MD, RD, AD) were found with the red nucleus across many different atlases.[32,33,37] Our results point towards a distributed network dysfunction hypothesis, in which the cerebellum, ventral posterior thalamus, red nucleus and brainstem nuclei (including the pedunculo-pontine nucleus) are involved in ET vulnerability. The grey and white matter alterations identified here implicate the entire network of regions targeted by DBS for the treatment of ET.

Cortical and Subcortical Volume Associations are Consistent with Known ET Pathophysiology

ET PRS was associated with reduced grey matter volumes in several cortical and subcortical areas, most notably in almost all parts of the brainstem, cerebellum, diencephalon and putamen. These findings align with a recent study showing significant atrophy in the middle and inferior cerebellar peduncles, as well as atrophy of bilateral cerebellar grey matter in patients with ET compared to controls.[71] In other studies, grey matter changes were seen in several areas similar to our present findings, including: bilateral cerebellum, bilateral parietal lobes, right frontal lobe, and right insula, along with white matter changes in the midbrain, in both occipital lobes, and right frontal lobe.[72] Importantly, we found associations of ET PRS with grey matter dMRI in various regions of the functional thalamus, the red nucleus, pons, brainstem, medulla, and ventral DC which incorporate regions interconnected by the prelemniscal, cortico-pontine, and dentato-rubro-thalamic tracts in the Guillain-Mollaret triangle, a circuit that coordinates cerebellar and cortical motor activity for fine motor control, and where lesions may cause tremor and other movement disorders.[6] Functional connectivity studies on patients with ET have also shown altered connectivity patterns between the cerebellum, thalamus, and several motor areas.[73] Specifically, resting state fMRI show abnormal functional connectivity within the cerebellar–thalamic–cortical network[74,75] and decreased functional connectivity locally within the cerebellum in patients with ET.[66,76] The cerebellar areas associated with ET PRS from the probabilistic tractography atlas are consistent with two distinct motor functional gradients, one located in area VI (1st motor functional gradient) and a 2nd motor representation covered by areas VIIB, VIIIA, VIIIB.[16] We found the strongest associations in all three areas of the 2nd motor functional gradient, in particular VIIb and VIIIa, which correspond to hand areas.[77] These areas mainly project to the dentate nucleus.[78]

medRxiv preprint doi: https://doi.org/10.1101/2024.07.16.24310501; this version posted July 16, 2024. The copyright holder for this preprint (which was not certified by peer review) is the author/funder, who has granted medRxiv a license to display the preprint in perpetuity. All rights reserved. No reuse allowed without permission.

Regions implicated in ET PRS are also affected in people diagnosed with ET

Examining ET through the liability threshold model provides a valuable framework where calculated PRS represents a normal distribution of ET specific genetic risk across a population. In this distribution of genetic risk, healthy individuals with low PRS will likely never manifest ET and carry little to no genetic vulnerability towards ET, making them near ideal controls. This is in contrast to individuals with high PRS, who have a higher likelihood of developing ET, but have not manifested symptoms. We therefore compared the microstructure of ET patients in the UKB to that of low-risk healthy controls. As expected, multiple grey matter volume reductions were observed in cerebellar regions of ET patients compared to low-risk individuals. Conversely, when comparing ET patients to high-risk healthy individuals, shared regions were affected in both groups. Microstructural alterations that are common between patients and high-risk individuals may be necessary for the development of ET but insufficient to cause ET alone. Differences between ET patients and high-risk healthy individuals may represent regions that must be additionally affected for ET to develop. However, note that the number of ET patients is small, limiting power. It is possible that additional disease associated common variants, rare variants, and environmental exposures are responsible for the observed differences between patients and high-risk individuals that push individuals past the liability threshold for ET. In the cerebellum, there are only three regions that are different between the high-risk healthy controls and the ET patients, those being the right VIIIa, the left I2IV, and the vermis CrusI, which suggests these regions may be important in the manifestation of ET. Also, differences in the pallidum and putamen and other regions are also observed between high-risk healthy individuals and patients. These differences may also play a role in the emergence of disease. Our results show that volume differences in the cerebellum are more widespread in the group of ET patients versus low-risk PRS in comparison to the group of ET patients versus high-risk PRS and suggests that genetically informed participant selection (low-risk vs high-risk 5% quantiles) reveals an ET phenotype gradient.

Shared Transcriptomics of Cerebellar Abnormalities Related to ET Identifies Several Genes in the 17q21.31 Locus of Chromosome 17

Using the ROIs associated with ET PRS, we used summary statistics from GWASes of corresponding grey matter volume IDPs to identify genes relevant to ET morphometry using GenomicSEM.[56,58] This yielded a list of 16 genes significantly associated with the latent variable representing ET vulnerability

medRxiv preprint doi: https://doi.org/10.1101/2024.07.16.24310501; this version posted July 16, 2024. The copyright holder for this preprint (which was not certified by peer review) is the author/funder, who has granted medRxiv a license to display the preprint in perpetuity. All rights reserved. No reuse allowed without permission.

in the cerebellum after Bonferroni correction ($p < 8.23e-6$). Of these genes, the identified ADP ribosylation factor like GTPase 17A coding gene *ARL17A* (p-value: 1.33e-06) was recently identified as an ET candidate gene in a whole genome sequencing study of familial ET.[79] Notably, the 17q21.31 locus encompassed roughly a third (5/16) of the identified genes in our transcriptomic analyses (Table S26). As such, the 17q21.31 locus, previously associated in multi-generational familial ET, may play a role in conferring structural brain susceptibilities in ET.[79] It is interesting to note that the 17q21.31 locus has been implicated in brain development and neurodegenerative disease.[80-83]

Limitations

Some limitations of this study include the universality and applicability of the PRS. Since the GWAS used to calculate PRS from was conducted only in European samples, the PRS is only accurate in European populations and does not hold in other populations. Through associating MRI measures with PRS as a proxy for genetic risk, we can only examine the consequence of SNPs which were included in the GWAS, which means other larger or rarer variant types such as structural copy number variants, repeat expansions, or translocations are not analysed. Some limitations that exist in the use of GenomicSEM and T-SEM is that we must maintain the use of European only data and we can only study the transcriptome of SNPs which are simultaneously reported in the phenotype GWASes of interest, the linkage reference dataset, and the GTEx expression reference dataset. As datasets expand, and as more diverse genomes are studies, these limitations will eventually be diminished.

Another limitation of this study is that it is cross-sectional in nature, limiting our ability to assess developmental or neurodegenerative trajectories related to ET PRS. Also, ET is a heterogeneous disorder, which may diminish the predictive power of the PRS. For example, many people with ET phenotype present additional neurological findings, a syndrome referred to as ET-plus. ET patients can also develop a parkinsonian syndrome. There are a number of ET phenotypic variants that may include different pathophysiology. Indeed, cerebellar volume differences between healthy controls and ET patients have been shown to differ substantially between different motor variants, with patients manifesting head tremors having greater differences in cerebellar volume versus healthy controls than ET patients manifesting with arm-tremors.[84] The lack of longitudinal data on included individuals prevents us from knowing if they eventually develop ET, ET with additional neurological signs, some other disorder entirely, or in fact remain healthy their entire lives.

medRxiv preprint doi: https://doi.org/10.1101/2024.07.16.24310501; this version posted July 16, 2024. The copyright holder for this preprint (which was not certified by peer review) is the author/funder, who has granted medRxiv a license to display the preprint in perpetuity. All rights reserved. No reuse allowed without permission.

Finally, in the analysis comparing ET patients to healthy controls of high and low genetic risk for ET, the sample size of patients are rather small. This creates a limitation of power and generalizability as we match controls to the age and sex of this patient sample set to control for potential confounders.

Conclusion

To better understand the associations between regional brain microstructure and ET we examined the correlation between ET PRS and neuroimaging measures in a large dataset of healthy adults. Recent advances in neuroimaging techniques, such as dMRI and morphometry, have provided valuable insights into the connections and structural alterations in the regions involved in ET. However, these studies could not address the question of the mechanism by which genetic risk leads to vulnerability. The literature lacks consensus on ET brain vulnerabilities, as neuroimaging findings in numerous ET studies reveal inconsistencies, suggesting a degree of heterogeneity.[85] Though several studies report cerebellar atrophy, some report hypertrophy, while others find no differences at all.[85] In our study, we quantify genetic risk via PRS to pinpoint structural vulnerabilities due to underlying ET specific genetic risk. ET is a complex disorder influenced by both environmental and genetic factors.[1] As we interrogate the genetic component of ET risk, we can examine brain vulnerabilities through a more focused lens, alleviating some of the variability seen in earlier studies as we narrow in on the consequence of aggregated ET genetic risk. In this ET PRS association study, we have identified white and grey matter vulnerabilities in healthy people genetically at risk of developing ET. We have found that most regions associated with ET PRS are part of a known motor network involved in ET pathogenesis, based on MRI studies and the functional neuroanatomy of DBS surgery. Additionally, we found genetic associations between regions of vulnerability in ET and the 17q21.31 locus. Of particular interest within this locus is the *ARL17A* gene, which represents a rare instance of a replicated candidate gene in ET.[79] Additionally, the 17q21.31 locus also harbors genes associated to neurodegenerative and neurodevelopmental phenotypes.[80-83] These findings suggest that ET vulnerability may depend on neurodevelopmental or neurodegenerative processes under genetic control.

Our work may also shed light on nonmotor clinical features of ET. ET is associated with depression and anxiety,[86,87] and genetically correlated with major depressive disorder.[3] Our ET PRS associations with IDPs also implicated prefrontal and orbitofrontal association tracts supports the hypothesis that ET is a complex disorder involving non-motor features including cognitive and psychiatric traits.[88-91] Non-motor regional vulnerabilities in unaffected individuals with heightened genetic risk of ET also supports the

medRxiv preprint doi: https://doi.org/10.1101/2024.07.16.24310501; this version posted July 16, 2024. The copyright holder for this preprint (which was not certified by peer review) is the author/funder, who has granted medRxiv a license to display the preprint in perpetuity. All rights reserved. No reuse allowed without permission.

idea that non-motor features might predate motor manifestations in ET.[89,91] Future research should focus on elucidating the precise mechanisms by which these structural alterations contribute to ET progression (prodromal ET), in comparison with other comorbid motor disorders (e.g. PD). Longitudinal studies of individuals with heightened genetic risk for ET may also be useful to discern the causes versus the consequences of disease. Together, this may ultimately pave the way for more effective diagnostic, and therapeutic approaches for this common movement disorder.

Data Availability

Genotyping and neuroimaging data are available through the UKB: https://www.ukbiobank.ac.uk/

Full ET summary statistics can be requested through 23andMe:
https://research.23andme.com/collaborate/#dataset-access/

Summary statistics for UKB brain imaging phenotypes can be accessed through BIG40:
https://open.win.ox.ac.uk/ukbiobank/big40/

GTEx datasets are available through: https://gtexportal.org/home/downloads/adult-gtex

The code used for analysis is accessible in the following repositories, which are publicly available.

PRS-CS is available via github repository: https://github.com/getian107/PRScs

PLINK is available via: http://pngu.mgh.harvard.edu/purcell/plink/

LDSC is available via github repository: https://github.com/bulik/ldsc

GenomicSEM is available via github repository: https://github.com/GenomicSEM/GenomicSEM

FUSION is available via: http://gusevlab.org/projects/fusion/

The WM dMRI code for the processing pipeline and containerized image are available in:

Pastor-Bernier, Alex (2022). White matter pipeline Singularity Image

Zenodo: https://zenodo.org/records/5910831

Github: https://github.com/hayabusapb/wma_qc

The GM dMRI code for the processing pipeline is available in:

Github: https://github.com/HoumanAzizi/UKB_DTI_Pipeline

medRxiv preprint doi: https://doi.org/10.1101/2024.07.16.24310501; this version posted July 16, 2024. The copyright holder for this preprint (which was not certified by peer review) is the author/funder, who has granted medRxiv a license to display the preprint in perpetuity. All rights reserved. No reuse allowed without permission.

Acknowledgements

We are thankful to the Rouleau lab members, and Filip Morys, Christina Tremblay, Lang Liu, Mari Shishikura, and Andrew Vo for their feedback and support. This work was supported by the Canadian Institutes of Health Research. We would also like to thank the employees and research participants of 23andMe, Inc. for making this work possible. This research used the NeuroHub infrastructure and was undertaken thanks in part to funding from the Canada First Research Excellence Fund, awarded through the Healthy Brains, Healthy Lives initiative at McGill University. This research was enabled in part by support provided by Calcul Québec and the Digital Research Alliance of Canada. This research has been conducted using the UK Biobank Resource under Application Number 45551.

Funding

MM received a doctoral student fellowship from the Canadian Institutes of Health Research (CIHR) (FRN193300) and a masters fellowship from the Fonds de Recherche Québec-Santé (303395). HA received a master's fellowship from the Fonds de Recherche Québec-Santé. ZS received a doctoral student fellowship from the Canadian Institutes of Health Research (CIHR) Frederick Banting & Charles Best Canada Graduate Scholarship (FRN260055) and the Transforming Autism Care Consortium, a thematic network supported by the Fonds de Recherche Québec-Santé. CEC received a doctoral student fellowship from the Canadian Institutes of Health Research (CIHR) (FBD187682). The Rouleau lab had support from the CIHR Foundation Award. The Dagher lab had support from (1) CIHR Foundation Award, and (2) Joint Programme – Neurodegenerative Disease.

medRxiv preprint doi: https://doi.org/10.1101/2024.07.16.24310501; this version posted July 16, 2024. The copyright holder for this preprint (which was not certified by peer review) is the author/funder, who has granted medRxiv a license to display the preprint in perpetuity. All rights reserved. No reuse allowed without permission.

References:

1. Welton T, Cardoso F, Carr JA, et al. Essential tremor. *Nat Rev Dis Primers*. Nov 11 2021;7(1):83. doi:10.1038/s41572-021-00314-w
2. Haubenberger D, Hallett M. Essential Tremor. *N Engl J Med*. Aug 9 2018;379(6):596-597. doi:10.1056/NEJMc1807690
3. Liao C, Castonguay CE, Heilbron K, et al. Association of Essential Tremor With Novel Risk Loci: A Genome-Wide Association Study and Meta-analysis. *JAMA Neurol*. Feb 1 2022;79(2):185-193. doi:10.1001/jamaneurol.2021.4781
4. Sudlow C, Gallacher J, Allen N, et al. UK biobank: an open access resource for identifying the causes of a wide range of complex diseases of middle and old age. *PLoS Med*. Mar 2015;12(3):e1001779. doi:10.1371/journal.pmed.1001779
5. Ge T, Chen CY, Ni Y, Feng YA, Smoller JW. Polygenic prediction via Bayesian regression and continuous shrinkage priors. *Nat Commun*. Apr 16 2019;10(1):1776. doi:10.1038/s41467-019-09718-5
6. Ogut E, Armagan K, Tufekci D. The Guillain-Mollaret triangle: a key player in motor coordination and control with implications for neurological disorders. *Neurosurg Rev*. Jul 20 2023;46(1):181. doi:10.1007/s10143-023-02086-1
7. Alfaro-Almagro F, Jenkinson M, Bangerter NK, et al. Image processing and Quality Control for the first 10,000 brain imaging datasets from UK Biobank. *Neuroimage*. Feb 1 2018;166:400-424. doi:10.1016/j.neuroimage.2017.10.034
8. Smith SM. Fast robust automated brain extraction. *Hum Brain Mapp*. Nov 2002;17(3):143-55. doi:10.1002/hbm.10062
9. Jenkinson M, Smith S. A global optimisation method for robust affine registration of brain images. *Med Image Anal*. Jun 2001;5(2):143-56. doi:10.1016/s1361-8415(01)00036-6
10. Jenkinson M, Bannister P, Brady M, Smith S. Improved optimization for the robust and accurate linear registration and motion correction of brain images. *Neuroimage*. Oct 2002;17(2):825-41. doi:10.1016/s1053-8119(02)91132-8
11. Zhang Y, Brady M, Smith S. Segmentation of brain MR images through a hidden Markov random field model and the expectation-maximization algorithm. *IEEE Trans Med Imaging*. Jan 2001;20(1):45-57. doi:10.1109/42.906424
12. Makris N, Goldstein JM, Kennedy D, et al. Decreased volume of left and total anterior insular lobule in schizophrenia. *Schizophr Res*. Apr 2006;83(2-3):155-71. doi:10.1016/j.schres.2005.11.020
13. Frazier JA, Chiu S, Breeze JL, et al. Structural brain magnetic resonance imaging of limbic and thalamic volumes in pediatric bipolar disorder. *Am J Psychiatry*. Jul 2005;162(7):1256-65. doi:10.1176/appi.ajp.162.7.1256
14. Desikan RS, Segonne F, Fischl B, et al. An automated labeling system for subdividing the human cerebral cortex on MRI scans into gyral based regions of interest. *Neuroimage*. Jul 1 2006;31(3):968-80. doi:10.1016/j.neuroimage.2006.01.021
15. Goldstein JM, Seidman LJ, Makris N, et al. Hypothalamic abnormalities in schizophrenia: sex effects and genetic vulnerability. *Biol Psychiatry*. Apr 15 2007;61(8):935-45. doi:10.1016/j.biopsych.2006.06.027
16. Diedrichsen J, Balsters JH, Flavell J, Cussans E, Ramnani N. A probabilistic MR atlas of the human cerebellum. *Neuroimage*. May 15 2009;46(1):39-46. doi:10.1016/j.neuroimage.2009.01.045
17. Dale AM, Fischl B, Sereno MI. Cortical surface-based analysis. I. Segmentation and surface reconstruction. *Neuroimage*. Feb 1999;9(2):179-94. doi:10.1006/nimg.1998.0395
18. Fischl B, Sereno MI, Dale AM. Cortical surface-based analysis. II: Inflation, flattening, and a surface-based coordinate system. *Neuroimage*. Feb 1999;9(2):195-207. doi:10.1006/nimg.1998.0396

medRxiv preprint doi: https://doi.org/10.1101/2024.07.16.24310501; this version posted July 16, 2024. The copyright holder for this preprint (which was not certified by peer review) is the author/funder, who has granted medRxiv a license to display the preprint in perpetuity. All rights reserved. No reuse allowed without permission.

19. Fischl B, Sereno MI, Tootell RB, Dale AM. High-resolution intersubject averaging and a coordinate system for the cortical surface. *Hum Brain Mapp*. 1999;8(4):272-84. doi:10.1002/(sici)1097-0193(1999)8:4<272::aid-hbm10>3.0.co;2-4
20. Fischl B, van der Kouwe A, Destrieux C, et al. Automatically parcellating the human cerebral cortex. *Cereb Cortex*. Jan 2004;14(1):11-22. doi:10.1093/cercor/bhg087
21. Iglesias JE, Augustinack JC, Nguyen K, et al. A computational atlas of the hippocampal formation using ex vivo, ultra-high resolution MRI: Application to adaptive segmentation of in vivo MRI. *Neuroimage*. Jul 15 2015;115:117-37. doi:10.1016/j.neuroimage.2015.04.042
22. Klapwijk ET, van de Kamp F, van der Meulen M, Peters S, Wierenga LM. Qoala-T: A supervised-learning tool for quality control of FreeSurfer segmented MRI data. *Neuroimage*. Apr 1 2019;189:116-129. doi:10.1016/j.neuroimage.2019.01.014
23. Alfaro-Almagro F, McCarthy P, Afyouni S, et al. Confound modelling in UK Biobank brain imaging. *Neuroimage*. Jan 1 2021;224:117002. doi:10.1016/j.neuroimage.2020.117002
24. Theaud G, Houde JC, Bore A, Rheault F, Morency F, Descoteaux M. TractoFlow: A robust, efficient and reproducible diffusion MRI pipeline leveraging Nextflow & Singularity. *Neuroimage*. Sep 2020;218:116889. doi:10.1016/j.neuroimage.2020.116889
25. Girard G, Whittingstall K, Deriche R, Descoteaux M. Towards quantitative connectivity analysis: reducing tractography biases. *Neuroimage*. Sep 2014;98:266-78. doi:10.1016/j.neuroimage.2014.04.074
26. Pasternak O, Sochen N, Gur Y, Intrator N, Assaf Y. Free water elimination and mapping from diffusion MRI. *Magn Reson Med*. Sep 2009;62(3):717-30. doi:10.1002/mrm.22055
27. Basser PJ, Pierpaoli C. Microstructural and physiological features of tissues elucidated by quantitative-diffusion-tensor MRI. *J Magn Reson B*. Jun 1996;111(3):209-19. doi:10.1006/jmrb.1996.0086
28. de Groot M, Vernooij MW, Klein S, et al. Improving alignment in Tract-based spatial statistics: evaluation and optimization of image registration. *Neuroimage*. Aug 1 2013;76:400-11. doi:10.1016/j.neuroimage.2013.03.015
29. Pastor-Bernier A. Singularity Image - wma_pipeline.
30. Horn A, Kuhn AA. Lead-DBS: a toolbox for deep brain stimulation electrode localizations and visualizations. *Neuroimage*. Feb 15 2015;107:127-135. doi:10.1016/j.neuroimage.2014.12.002
31. Zhang Y, Larcher KM, Misic B, Dagher A. Anatomical and functional organization of the human substantia nigra and its connections. *Elife*. Aug 21 2017;6doi:10.7554/eLife.26653
32. Nowacki A, Barlatey S, Al-Fatly B, et al. Probabilistic Mapping Reveals Optimal Stimulation Site in Essential Tremor. *Ann Neurol*. May 2022;91(5):602-612. doi:10.1002/ana.26324
33. Neudorfer C, Kroneberg D, Al-Fatly B, et al. Personalizing Deep Brain Stimulation Using Advanced Imaging Sequences. *Ann Neurol*. May 2022;91(5):613-628. doi:10.1002/ana.26326
34. Horn A, Kuhn AA, Merkl A, Shih L, Alterman R, Fox M. Probabilistic conversion of neurosurgical DBS electrode coordinates into MNI space. *Neuroimage*. Apr 15 2017;150:395-404. doi:10.1016/j.neuroimage.2017.02.004
35. Middlebrooks EH, Domingo RA, Vivas-Buitrago T, et al. Neuroimaging Advances in Deep Brain Stimulation: Review of Indications, Anatomy, and Brain Connectomics. *AJNR Am J Neuroradiol*. Sep 2020;41(9):1558-1568. doi:10.3174/ajnr.A6693
36. Horn A, Reich MM, Ewert S, et al. Optimal deep brain stimulation sites and networks for cervical vs. generalized dystonia. *Proc Natl Acad Sci U S A*. Apr 5 2022;119(14):e2114985119. doi:10.1073/pnas.2114985119
37. Neudorfer C, Germann J, Elias GJB, Gramer R, Boutet A, Lozano AM. A high-resolution in vivo magnetic resonance imaging atlas of the human hypothalamic region. *Sci Data*. Sep 15 2020;7(1):305. doi:10.1038/s41597-020-00644-6

medRxiv preprint doi: https://doi.org/10.1101/2024.07.16.24310501; this version posted July 16, 2024. The copyright holder for this preprint (which was not certified by peer review) is the author/funder, who has granted medRxiv a license to display the preprint in perpetuity. All rights reserved. No reuse allowed without permission.

38. Boutet A, Germann J, Gwun D, et al. Sign-specific stimulation 'hot' and 'cold' spots in Parkinson's disease validated with machine learning. *Brain Commun*. 2021;3(2):fcab027. doi:10.1093/braincomms/fcab027
39. Kumar VJ, van Oort E, Scheffler K, Beckmann CF, Grodd W. Functional anatomy of the human thalamus at rest. *Neuroimage*. Feb 15 2017;147:678-691. doi:10.1016/j.neuroimage.2016.12.071
40. Elias GJB, Boutet A, Joel SE, et al. Probabilistic Mapping of Deep Brain Stimulation: Insights from 15 Years of Therapy. *Ann Neurol*. Mar 2021;89(3):426-443. doi:10.1002/ana.25975
41. Choi EY, Yeo BT, Buckner RL. The organization of the human striatum estimated by intrinsic functional connectivity. *J Neurophysiol*. Oct 2012;108(8):2242-63. doi:10.1152/jn.00270.2012
42. Tang Y, Sun W, Toga AW, Ringman JM, Shi Y. A probabilistic atlas of human brainstem pathways based on connectome imaging data. *Neuroimage*. Apr 1 2018;169:227-239. doi:10.1016/j.neuroimage.2017.12.042
43. Lau JC, Xiao Y, Haast RAM, et al. Direct visualization and characterization of the human zona incerta and surrounding structures. *Hum Brain Mapp*. Nov 2020;41(16):4500-4517. doi:10.1002/hbm.25137
44. Ewert S, Plettig P, Li N, et al. Toward defining deep brain stimulation targets in MNI space: A subcortical atlas based on multimodal MRI, histology and structural connectivity. *Neuroimage*. Apr 15 2018;170:271-282. doi:10.1016/j.neuroimage.2017.05.015
45. Ilinsky I, Horn A, Paul-Gilloteaux P, Gressens P, Verney C, Kultas-Ilinsky K. Human Motor Thalamus Reconstructed in 3D from Continuous Sagittal Sections with Identified Subcortical Afferent Territories. *eNeuro*. May-Jun 2018;5(3)doi:10.1523/ENEURO.0060-18.2018
46. Tian Y, Margulies DS, Breakspear M, Zalesky A. Topographic organization of the human subcortex unveiled with functional connectivity gradients. *Nat Neurosci*. Nov 2020;23(11):1421-1432. doi:10.1038/s41593-020-00711-6
47. Su JH, Thomas FT, Kasoff WS, et al. Thalamus Optimized Multi Atlas Segmentation (THOMAS): fast, fully automated segmentation of thalamic nuclei from structural MRI. *Neuroimage*. Jul 1 2019;194:272-282. doi:10.1016/j.neuroimage.2019.03.021
48. He X, Chaitanya G, Asma B, et al. Disrupted basal ganglia-thalamocortical loops in focal to bilateral tonic-clonic seizures. *Brain*. Jan 1 2020;143(1):175-190. doi:10.1093/brain/awz361
49. Alkemade A, Mulder MJ, Groot JM, et al. The Amsterdam Ultra-high field adult lifespan database (AHEAD): A freely available multimodal 7 Tesla submillimeter magnetic resonance imaging database. *Neuroimage*. Nov 1 2020;221:117200. doi:10.1016/j.neuroimage.2020.117200
50. Yu B, Li L, Guan X, et al. HybraPD atlas: Towards precise subcortical nuclei segmentation using multimodality medical images in patients with Parkinson disease. *Hum Brain Mapp*. Sep 2021;42(13):4399-4421. doi:10.1002/hbm.25556
51. Xiao Y, Lau JC, Anderson T, et al. An accurate registration of the BigBrain dataset with the MNI PD25 and ICBM152 atlases. *Sci Data*. Oct 17 2019;6(1):210. doi:10.1038/s41597-019-0217-0
52. Chang CC, Chow CC, Tellier LC, Vattikuti S, Purcell SM, Lee JJ. Second-generation PLINK: rising to the challenge of larger and richer datasets. *Gigascience*. 2015;4:7. doi:10.1186/s13742-015-0047-8
53. Collister JA, Liu X, Clifton L. Calculating Polygenic Risk Scores (PRS) in UK Biobank: A Practical Guide for Epidemiologists. *Front Genet*. 2022;13:818574. doi:10.3389/fgene.2022.818574
54. Genomes Project C, Auton A, Brooks LD, et al. A global reference for human genetic variation. *Nature*. Oct 1 2015;526(7571):68-74. doi:10.1038/nature15393
55. Ruxton GD. The unequal variance t-test is an underused alternative to Student's t-test and the Mann–Whitney U test. *Behavioral Ecology*. 2006;17(4):688-690. doi:10.1093/beheco/ark016
56. Grotzinger AD, Rhemtulla M, de Vlaming R, et al. Genomic structural equation modelling provides insights into the multivariate genetic architecture of complex traits. *Nat Hum Behav*. May 2019;3(5):513-525. doi:10.1038/s41562-019-0566-x

medRxiv preprint doi: https://doi.org/10.1101/2024.07.16.24310501; this version posted July 16, 2024. The copyright holder for this preprint (which was not certified by peer review) is the author/funder, who has granted medRxiv a license to display the preprint in perpetuity. All rights reserved. No reuse allowed without permission.

57. Bulik-Sullivan BK, Loh PR, Finucane HK, et al. LD Score regression distinguishes confounding from polygenicity in genome-wide association studies. *Nat Genet*. Mar 2015;47(3):291-5. doi:10.1038/ng.3211
58. Smith SM, Douaud G, Chen W, et al. An expanded set of genome-wide association studies of brain imaging phenotypes in UK Biobank. *Nature Neuroscience*. 2021/05/01 2021;24(5):737-745. doi:10.1038/s41593-021-00826-4
59. Gusev A, Ko A, Shi H, et al. Integrative approaches for large-scale transcriptome-wide association studies. *Nat Genet*. Mar 2016;48(3):245-52. doi:10.1038/ng.3506
60. Feng H, Mancuso N, Gusev A, et al. Leveraging expression from multiple tissues using sparse canonical correlation analysis and aggregate tests improves the power of transcriptome-wide association studies. *PLoS Genet*. Apr 2021;17(4):e1008973. doi:10.1371/journal.pgen.1008973
61. Zhang F, Wu Y, Norton I, et al. An anatomically curated fiber clustering white matter atlas for consistent white matter tract parcellation across the lifespan. *Neuroimage*. Oct 1 2018;179:429-447. doi:10.1016/j.neuroimage.2018.06.027
62. Buckner RL, Krienen FM, Castellanos A, Diaz JC, Yeo BT. The organization of the human cerebellum estimated by intrinsic functional connectivity. *J Neurophysiol*. Nov 2011;106(5):2322-45. doi:10.1152/jn.00339.2011
63. Thevathasan W, Debu B, Aziz T, et al. Pedunculopontine nucleus deep brain stimulation in Parkinson's disease: A clinical review. *Mov Disord*. Jan 2018;33(1):10-20. doi:10.1002/mds.27098
64. Nestrasil I, Svatkova A, Rudser KD, et al. White matter measures correlate with essential tremor severity-A pilot diffusion tensor imaging study. *Brain Behav*. Aug 2018;8(8):e01039. doi:10.1002/brb3.1039
65. Shin DH, Han BS, Kim HS, Lee PH. Diffusion tensor imaging in patients with essential tremor. *AJNR Am J Neuroradiol*. Jan 2008;29(1):151-3. doi:10.3174/ajnr.A0744
66. Saini J, Bagepally BS, Bhatt MD, et al. Diffusion tensor imaging: tract based spatial statistics study in essential tremor. *Parkinsonism Relat Disord*. Jun 2012;18(5):477-82. doi:10.1016/j.parkreldis.2012.01.006
67. Babij R, Lee M, Cortes E, Vonsattel JP, Faust PL, Louis ED. Purkinje cell axonal anatomy: quantifying morphometric changes in essential tremor versus control brains. *Brain*. Oct 2013;136(Pt 10):3051-61. doi:10.1093/brain/awt238
68. Louis ED. Essential tremor and the cerebellum. *Handb Clin Neurol*. 2018;155:245-258. doi:10.1016/B978-0-444-64189-2.00016-0
69. Choe M, Cortes E, Vonsattel JP, Kuo SH, Faust PL, Louis ED. Purkinje cell loss in essential tremor: Random sampling quantification and nearest neighbor analysis. *Mov Disord*. Mar 2016;31(3):393-401. doi:10.1002/mds.26490
70. Benito-Leon J, Mato-Abad V, Louis ED, et al. White matter microstructural changes are related to cognitive dysfunction in essential tremor. *Sci Rep*. Jun 7 2017;7(1):2978. doi:10.1038/s41598-017-02596-1
71. Prasad S, Pandey U, Saini J, Ingalhalikar M, Pal PK. Atrophy of cerebellar peduncles in essential tremor: a machine learning-based volumetric analysis. *Eur Radiol*. Dec 2019;29(12):7037-7046. doi:10.1007/s00330-019-06269-7
72. Benito-Leon J, Alvarez-Linera J, Hernandez-Tamames JA, Alonso-Navarro H, Jimenez-Jimenez FJ, Louis ED. Brain structural changes in essential tremor: voxel-based morphometry at 3-Tesla. *J Neurol Sci*. Dec 15 2009;287(1-2):138-42. doi:10.1016/j.jns.2009.08.037
73. Tikoo S, Pietracupa S, Tommasin S, et al. Functional disconnection of the dentate nucleus in essential tremor. *J Neurol*. May 2020;267(5):1358-1367. doi:10.1007/s00415-020-09711-9
74. Popa T, Russo M, Vidailhet M, et al. Cerebellar rTMS stimulation may induce prolonged clinical benefits in essential tremor, and subjacent changes in functional connectivity: an open label trial. *Brain Stimul*. Mar 2013;6(2):175-9. doi:10.1016/j.brs.2012.04.009

medRxiv preprint doi: https://doi.org/10.1101/2024.07.16.24310501; this version posted July 16, 2024. The copyright holder for this preprint (which was not certified by peer review) is the author/funder, who has granted medRxiv a license to display the preprint in perpetuity. All rights reserved. No reuse allowed without permission.

75. Nicoletti V, Cecchi P, Pesaresi I, Frosini D, Cosottini M, Ceravolo R. Cerebello-thalamo-cortical network is intrinsically altered in essential tremor: evidence from a resting state functional MRI study. *Sci Rep*. Oct 7 2020;10(1):16661. doi:10.1038/s41598-020-73714-9
76. Novellino F, Nicoletti G, Cherubini A, et al. Cerebellar involvement in essential tremor with and without resting tremor: A Diffusion Tensor Imaging study. *Parkinsonism Relat Disord*. Jun 2016;27:61-6. doi:10.1016/j.parkreldis.2016.03.022
77. Saadon-Grosman N, Angeli PA, DiNicola LM, Buckner RL. A third somatomotor representation in the human cerebellum. *J Neurophysiol*. Oct 1 2022;128(4):1051-1073. doi:10.1152/jn.00165.2022
78. Matano S. Brief communication: Proportions of the ventral half of the cerebellar dentate nucleus in humans and great apes. *Am J Phys Anthropol*. Feb 2001;114(2):163-5. doi:10.1002/1096-8644(200102)114:2<163::AID-AJPA1016>3.0.CO;2-F
79. Clark LN, Gao Y, Wang GT, et al. Whole genome sequencing identifies candidate genes for familial essential tremor and reveals biological pathways implicated in essential tremor aetiology. *EBioMedicine*. Nov 2022;85:104290. doi:10.1016/j.ebiom.2022.104290
80. Mahajan GJ, Vallender EJ, Garrett MR, et al. Altered neuro-inflammatory gene expression in hippocampus in major depressive disorder. *Prog Neuropsychopharmacol Biol Psychiatry*. Mar 2 2018;82:177-186. doi:10.1016/j.pnpbp.2017.11.017
81. Cheng W, van der Meer D, Parker N, et al. Shared genetic architecture between schizophrenia and subcortical brain volumes implicates early neurodevelopmental processes and brain development in childhood. *Mol Psychiatry*. Dec 2022;27(12):5167-5176. doi:10.1038/s41380-022-01751-z
82. Koolen DA, Vissers LE, Pfundt R, et al. A new chromosome 17q21.31 microdeletion syndrome associated with a common inversion polymorphism. *Nat Genet*. Sep 2006;38(9):999-1001. doi:10.1038/ng1853
83. Cervera-Carles L, Pagonabarraga J, Pascual-Sedano B, et al. Copy number variation analysis of the 17q21.31 region and its role in neurodegenerative diseases. *Am J Med Genet B Neuropsychiatr Genet*. Mar 2016;171B(2):175-80. doi:10.1002/ajmg.b.32390
84. Cerasa A, Messina D, Nicoletti G, et al. Cerebellar atrophy in essential tremor using an automated segmentation method. *AJNR Am J Neuroradiol*. Jun 2009;30(6):1240-3. doi:10.3174/ajnr.A1544
85. Wang Q, Aljassar M, Bhagwat N, et al. Reproducibility of cerebellar involvement as quantified by consensus structural MRI biomarkers in advanced essential tremor. *Sci Rep*. Jan 11 2023;13(1):581. doi:10.1038/s41598-022-25306-y
86. Gerbasi ME, Nambiar S, Reed S, et al. Essential tremor patients experience significant burden beyond tremor: A systematic literature review. *Front Neurol*. 2022;13:891446. doi:10.3389/fneur.2022.891446
87. Huang H, Yang X, Zhao Q, et al. Prevalence and Risk Factors of Depression and Anxiety in Essential Tremor Patients: A Cross-Sectional Study in Southwest China. *Front Neurol*. 2019;10:1194. doi:10.3389/fneur.2019.01194
88. Louis ED. Essential tremors: a family of neurodegenerative disorders? *Arch Neurol*. Oct 2009;66(10):1202-8. doi:10.1001/archneurol.2009.217
89. Louis ED. Non-motor symptoms in essential tremor: A review of the current data and state of the field. *Parkinsonism Relat Disord*. Jan 2016;22 Suppl 1(0 1):S115-8. doi:10.1016/j.parkreldis.2015.08.034
90. Louis ED. Essential tremor as a neuropsychiatric disorder. *J Neurol Sci*. Feb 15 2010;289(1-2):144-8. doi:10.1016/j.jns.2009.08.029
91. Jhunjhunwala K, Pal PK. The Non-motor Features of Essential Tremor: A Primary Disease Feature or Just a Secondary Phenomenon? *Tremor Other Hyperkinet Mov (N Y)*. 2014;4:255. doi:10.7916/D8D798MZ